

# Advances in single- and multiple-scattering simulation capabilities in support of polarimetric remote sensing of the atmosphere and oceans

Ping Yang\*, Jiachen Ding, and Masanori Saito

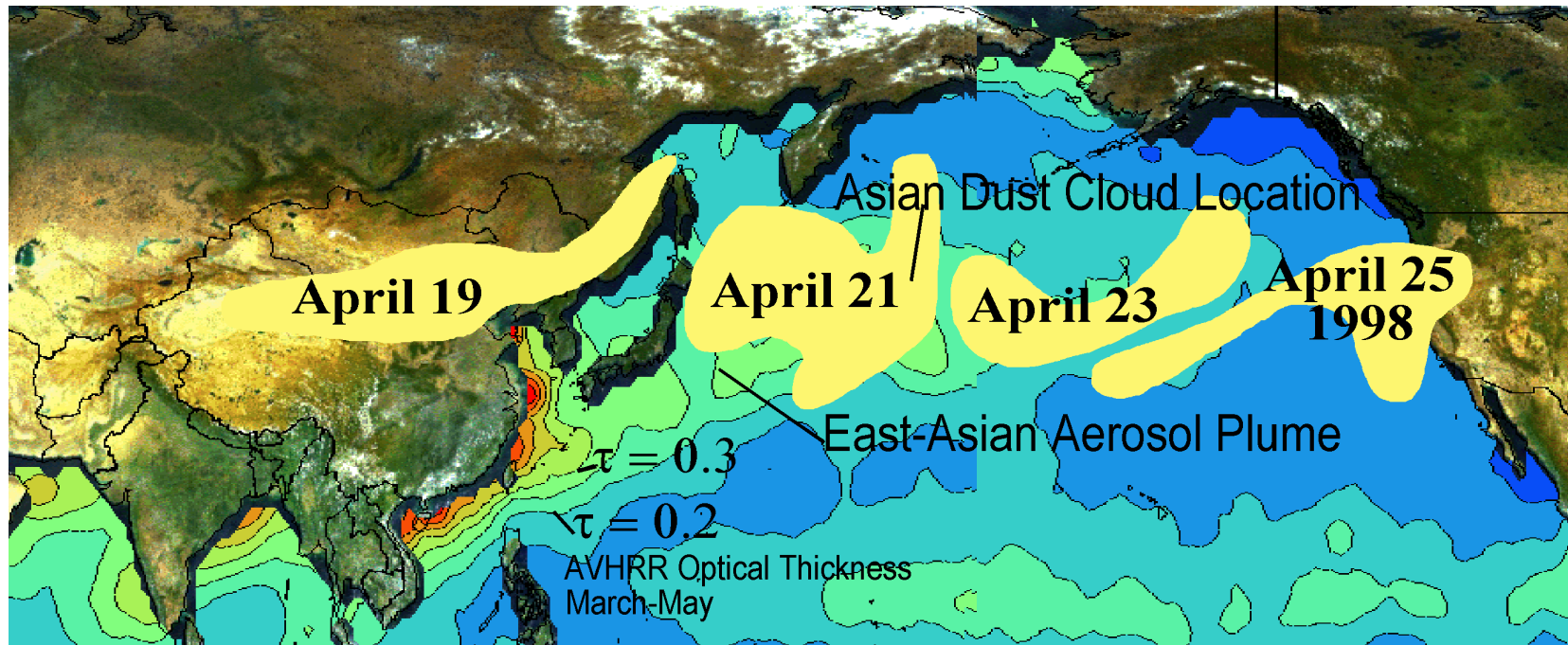
Department of Atmospheric Sciences, Texas A&M University, College Station, TX



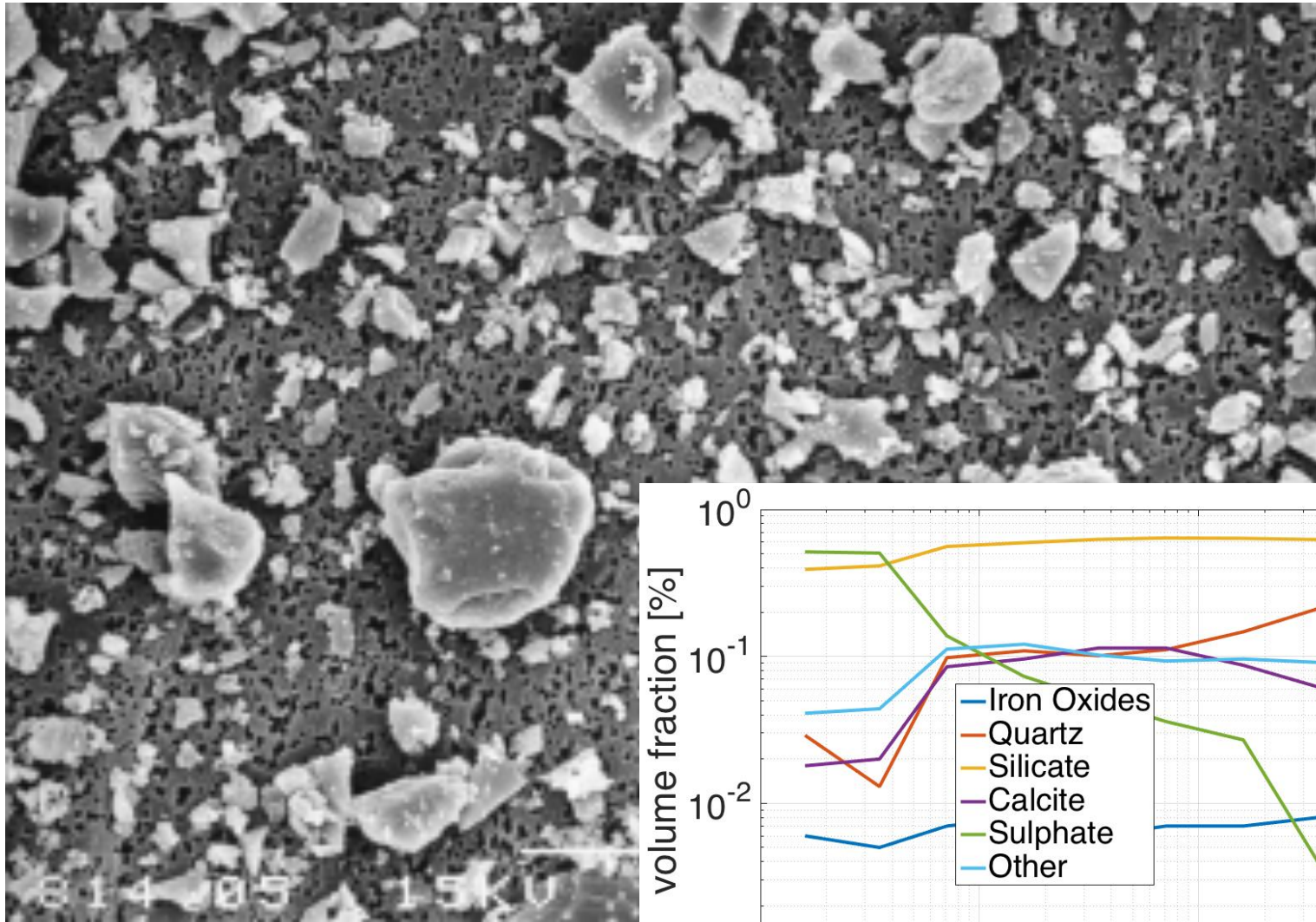
Dust storm in Phoenix, AZ on Aug. 2, 2018

# “Dust: Small-scale processes with global consequences” (Okin et al., 2011)

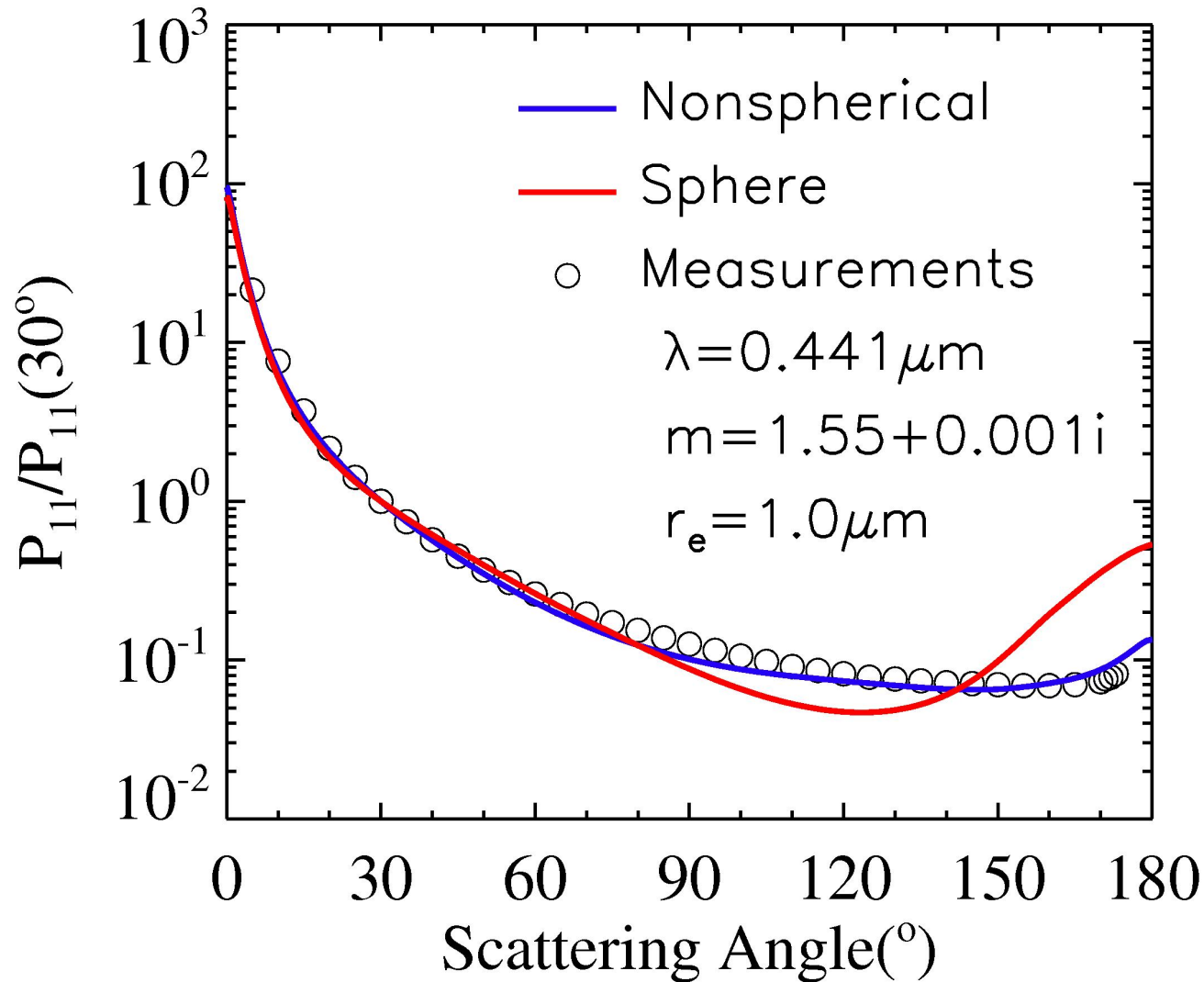
The track of a large dust storm that was followed with the SeaWiFS Satellite in 1998



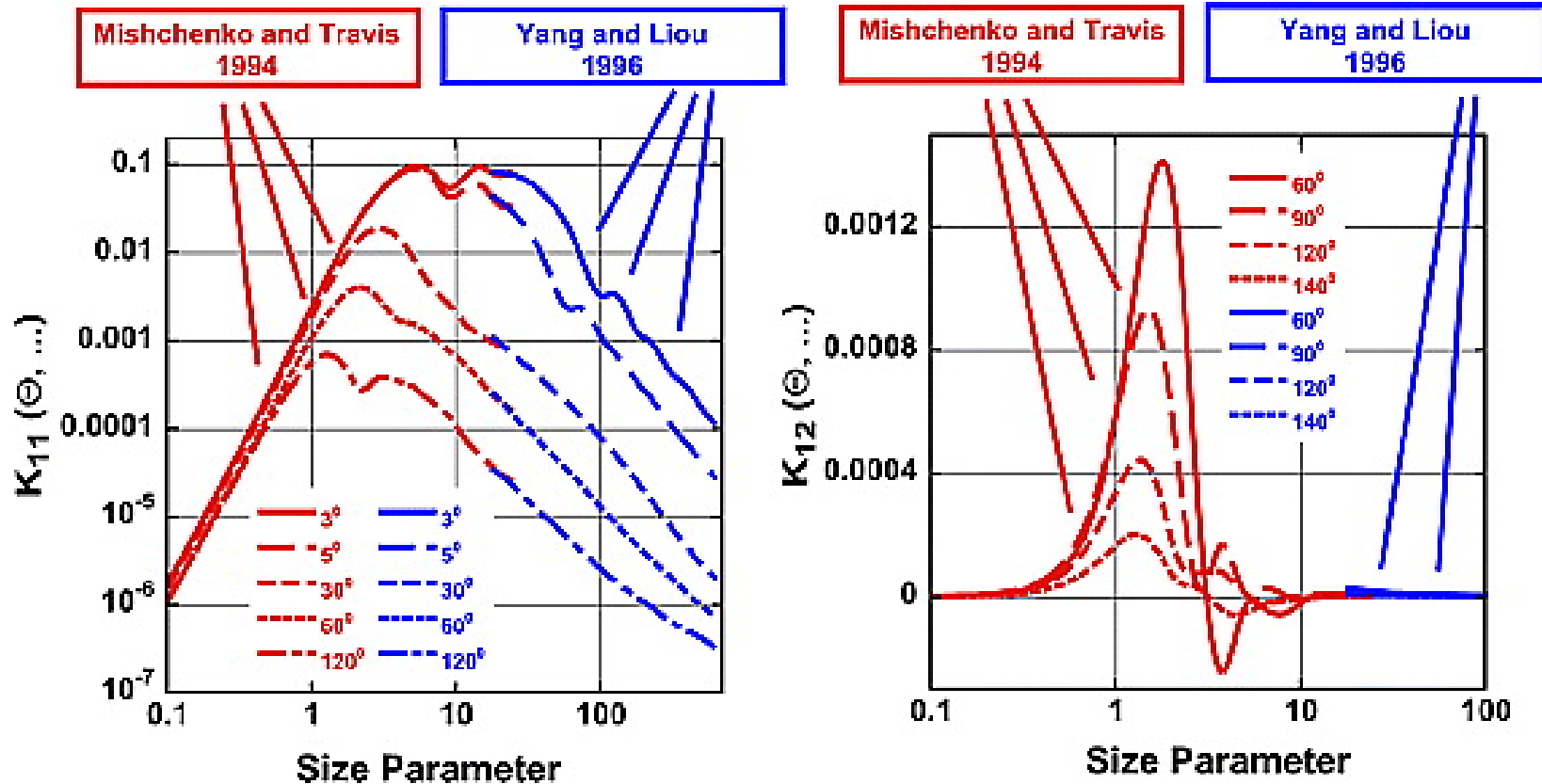
Source: R. B. Husar et al, JGR, 2001



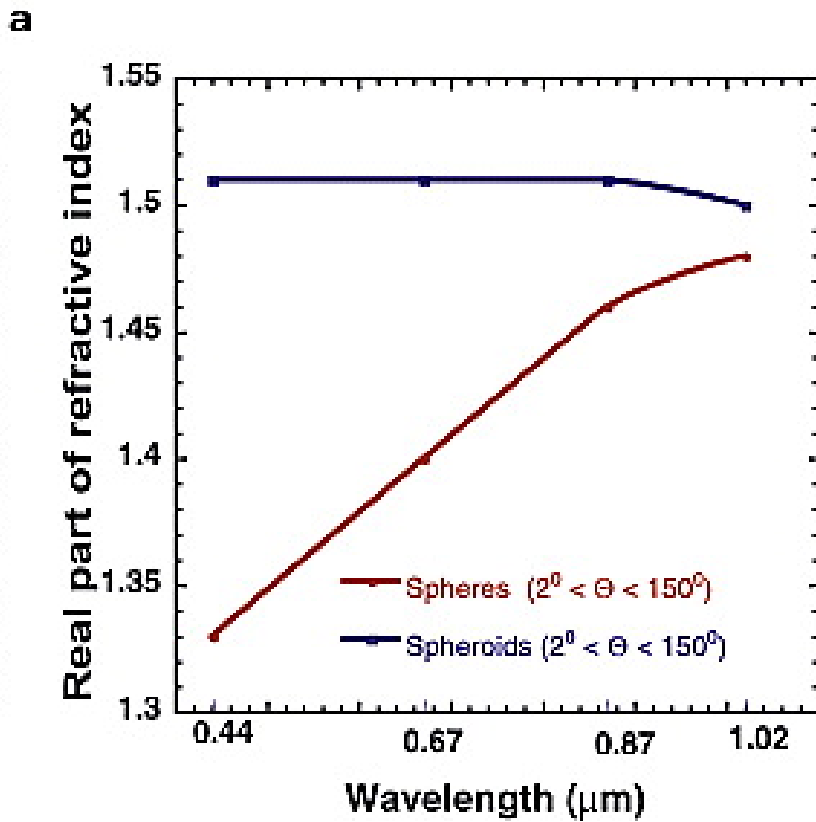
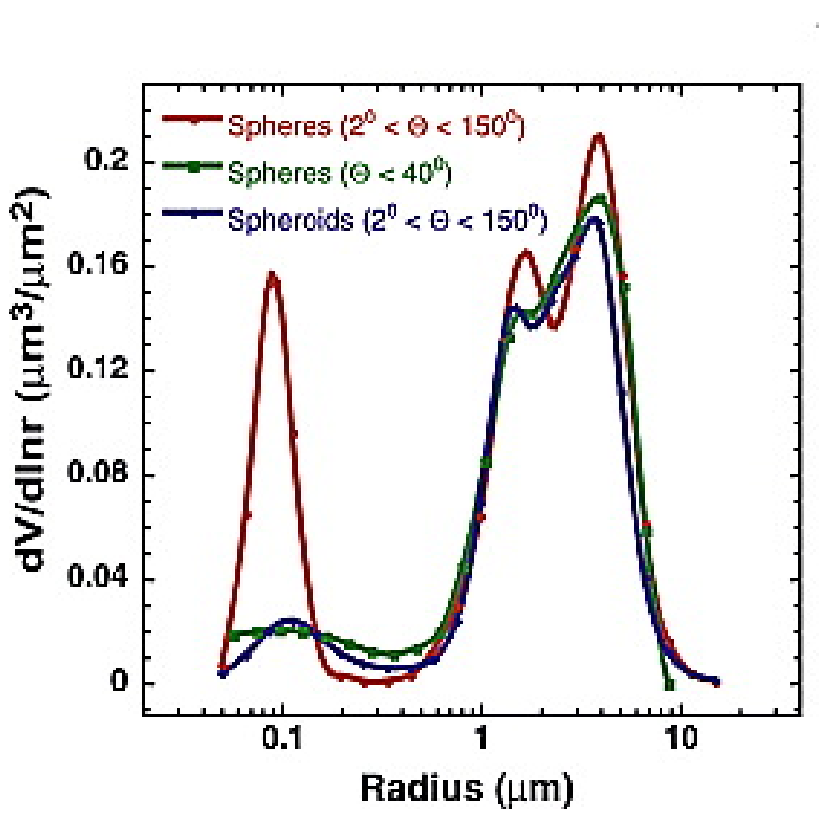
Mineral aerosols sample (feldspar) SEM image (Volten et al., 2001). Dust aerosols are exclusively irregular particles with arbitrary geometries.



Comparison between the phase functions computed for spherical and nonspherical dust particles (Feng, Yang, Kattawar, Hsu, Tsay and Laszlo, 2009). The symbols indicate laboratory measurements (Volten et al. 2001).



Elements of the kernel matrices  $K_{11}(\Theta, \lambda, n, k, p, rk)$  and  $K_{12}(\Theta, \lambda, n, k, p, rk)$  at different scattering angles for prolate randomly oriented spheroids ( $\epsilon = \sim 2.7$ ,  $n = 1.53 + i0.003$ ). The red and blue curves show the results obtained with the  $T$ -matrix code [Mishchenko and Travis, 1994] and the Yang and Liou [ 1996] method, respectively. *Adapted from Dubovik et al. (2006),*



A typical situation where utilizing the spheroid scattering assumption [[Dubovik et al., 2002b](#)] resulted in the removal of the false fine mode in the size distribution and false spectral dependence in the real part of refractive index. Size distributions and refractive indices are retrieved assuming sphere and spheroid models from spectral radiance measurements covering the full range of scattering angles. The size distribution retrieved from the aureole only ( $\Theta < 40^\circ$ , where effects of nonsphericity are minimal) and assuming spherical particles is also shown. *Adapted from Dubovik et al. (2006).*

# Objectives

In support of polarimetric remote sensing, we developed:

- Robust modeling capabilities to simulate the single-scattering properties of atmospheric particles (irregular dust particles and ice crystals)
- Efficient vector radiative transfer (RT) modeling capabilities for in-line RT simulations involved in active and passive remote sensing applications

# State-of-the-art light-scattering computational methods

- **Exact methods:**
  - Extended Boundary Condition T-matrix Method (EBCM)
  - Invariant Imbedding T-matrix Method (II-TM)
- **Approximate method:**  
Physical Geometric Optics Method (PGOM)

# T-matrix

- Expand the incident and scattered fields

$$\mathbf{E}^{\text{inc}}(\vec{r}) = \sum_{n=1}^{\infty} \sum_{m=-n}^n a_{mn} \mathbf{RgM}_{nm}(k\vec{r}) + b_{mn} \mathbf{RgN}_{nm}(k\vec{r})$$

$$\mathbf{E}^{\text{sca}}(\vec{r}) = \sum_{n=1}^{\infty} \sum_{m=-n}^n p_{mn} \mathbf{M}_{nm}(k\vec{r}) + q_{mn} \mathbf{N}_{nm}(k\vec{r})$$

- Connect the expansion coefficients via the T-matrix

$$\begin{pmatrix} \mathbf{p} \\ \mathbf{q} \end{pmatrix} = \begin{pmatrix} \mathbf{T}^{11} & \mathbf{T}^{12} \\ \mathbf{T}^{21} & \mathbf{T}^{22} \end{pmatrix} \begin{pmatrix} \mathbf{a} \\ \mathbf{b} \end{pmatrix}$$

- Compute the single-scattering properties via the T-matrix

$$\langle C_{ext} \rangle = -\frac{2\pi}{k^2} \sum_{n=1}^{\infty} \sum_{m=-n}^n \text{Re} \left( \mathbf{T}_{mn}^{11} + \mathbf{T}_{mn}^{22} \right)$$

$$\langle C_{sca} \rangle = \frac{2\pi}{k^2} \sum_{n=1}^{\infty} \sum_{m=-n}^n \sum_{n'=1}^{\infty} \sum_{m'=-n'}^n \left[ \left| \mathbf{T}_{mn'm'n'}^{11} \right|^2 + \left| \mathbf{T}_{mn'm'n'}^{12} \right|^2 + \left| \mathbf{T}_{mn'm'n'}^{21} \right|^2 + \left| \mathbf{T}_{mn'm'n'}^{22} \right|^2 \right]$$

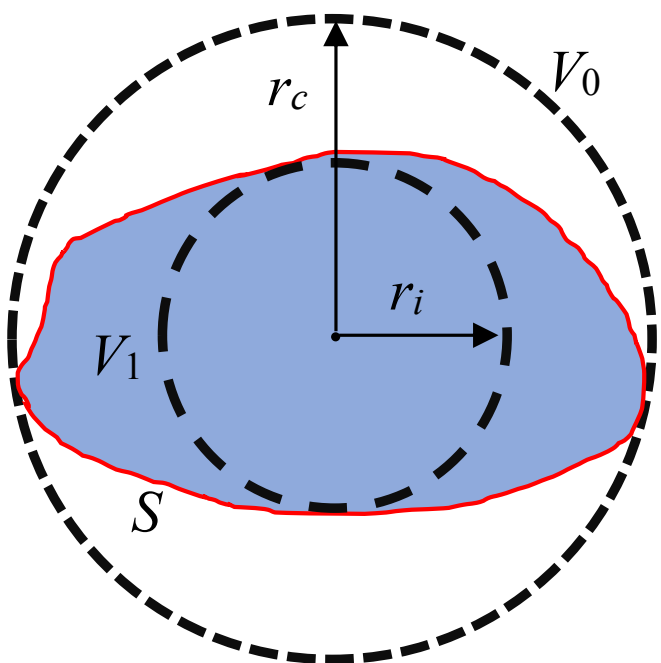
# Extended Boundary Condition T-matrix Method

(mathematically, a boundary-value problem)

Surface integrals

$$\mathbf{E}^{\text{sca}}(\vec{r}') = \oint_S dS \left\{ ik \left[ \hat{n}_s \times \mathbf{H}^{\text{int}}(\vec{r}) \right] \cdot \vec{G}(\vec{r}, \vec{r}') + \left[ \hat{n}_s \times \mathbf{E}^{\text{int}}(\vec{r}) \right] \cdot \left[ \nabla \times \vec{G}(\vec{r}, \vec{r}') \right] \right\}, \vec{r}' \in V_0,$$

$$\mathbf{E}^{\text{inc}}(\vec{r}') = - \oint_S dS \left\{ ik \left[ \hat{n}_s \times \mathbf{H}^{\text{int}}(\vec{r}) \right] \cdot \vec{G}(\vec{r}, \vec{r}') + \left[ \hat{n}_s \times \mathbf{E}^{\text{int}}(\vec{r}) \right] \cdot \left[ \nabla \times \vec{G}(\vec{r}, \vec{r}') \right] \right\}, \vec{r}' \in V_1,$$

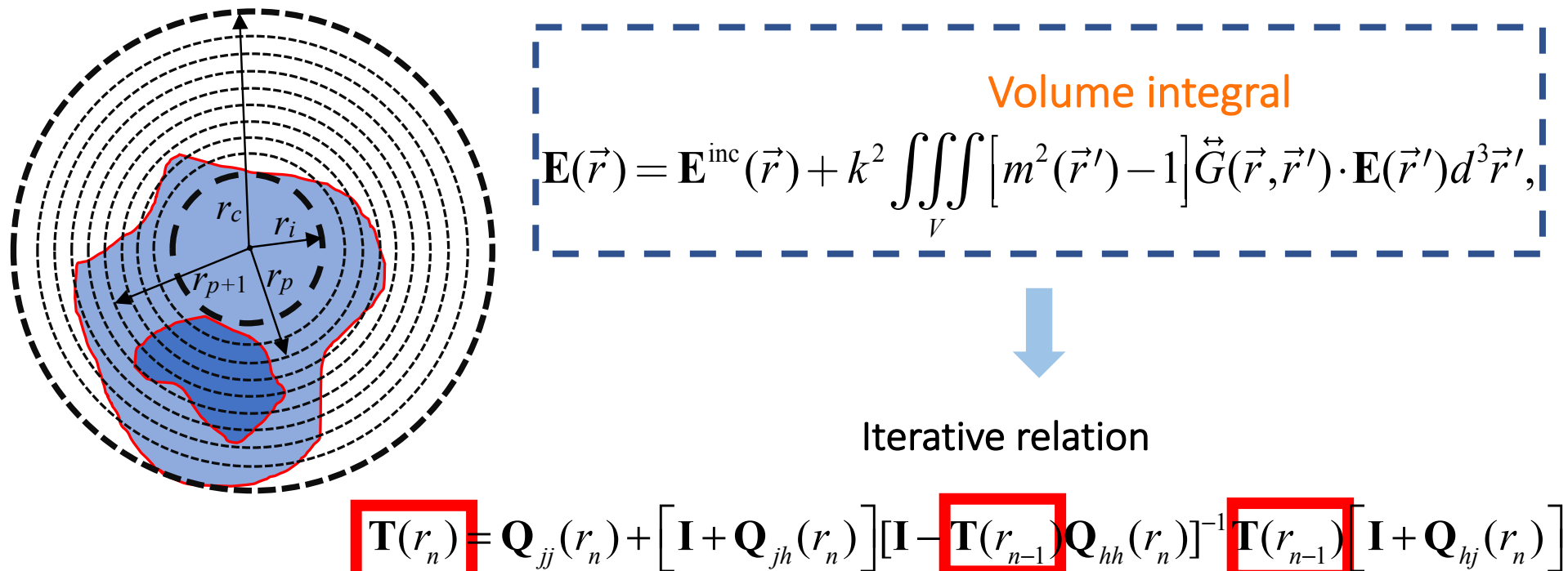


$$\begin{pmatrix} \mathbf{p} \\ \mathbf{q} \end{pmatrix} = -Rg\mathbf{Q} \begin{pmatrix} \mathbf{c} \\ \mathbf{d} \end{pmatrix}, \quad \begin{pmatrix} \mathbf{a} \\ \mathbf{b} \end{pmatrix} = \mathbf{Q} \begin{pmatrix} \mathbf{c} \\ \mathbf{d} \end{pmatrix},$$

$$\begin{pmatrix} \mathbf{p} \\ \mathbf{q} \end{pmatrix} = \mathbf{T} \begin{pmatrix} \mathbf{a} \\ \mathbf{b} \end{pmatrix}, \quad \mathbf{T} = -(\mathbf{RgQ})\mathbf{Q}^{-1}.$$

Waterman (1971); Mischenko and Travis, (1994); Tsang et al., (2000)

# Invariant Imbedding T-matrix (II-TM) Method (mathematically, an initial-value problem)



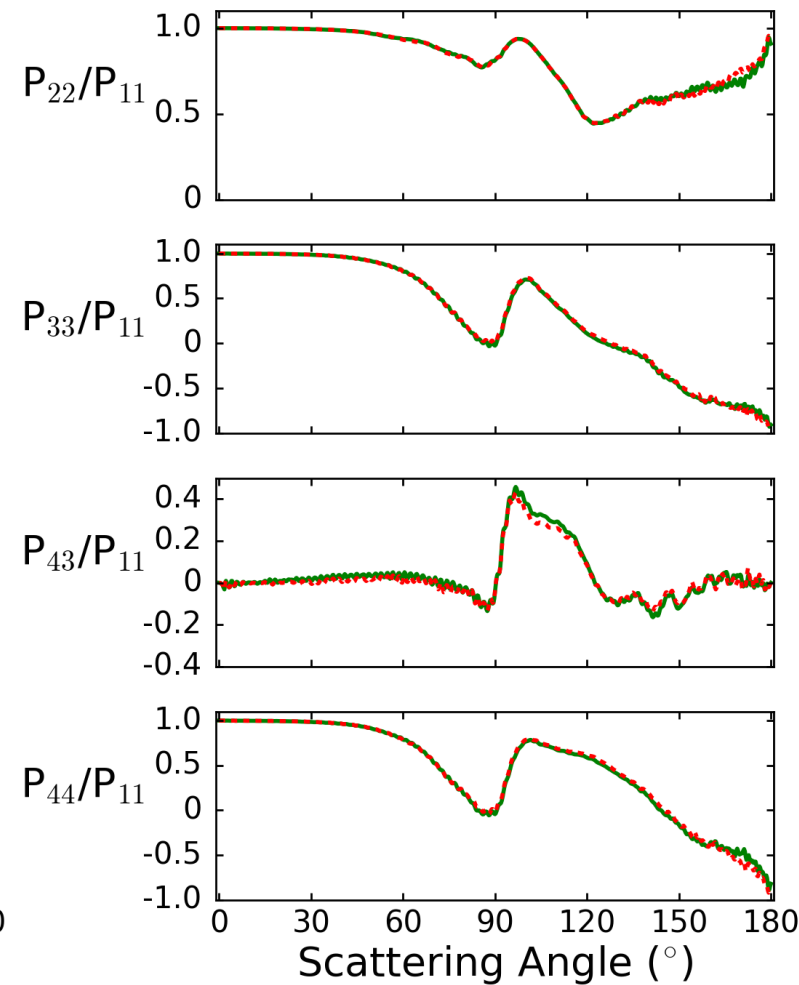
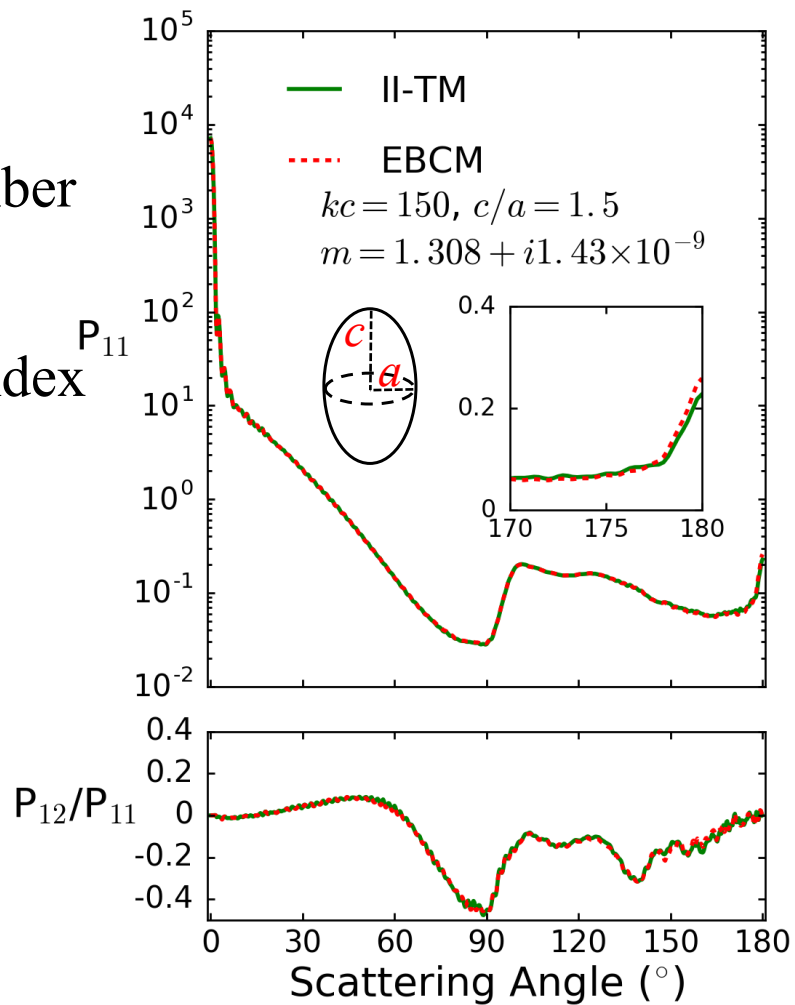
The  $\mathbf{Q}$  matrix is related to the particle shape and refractive index.

Johnson (1988); Bi, Yang, Kattawar, and Mishchenko (2013); Bi and Yang (2014)

## II-TM and EBCM comparison: nonabsorptive case

$k$ : wavenumber

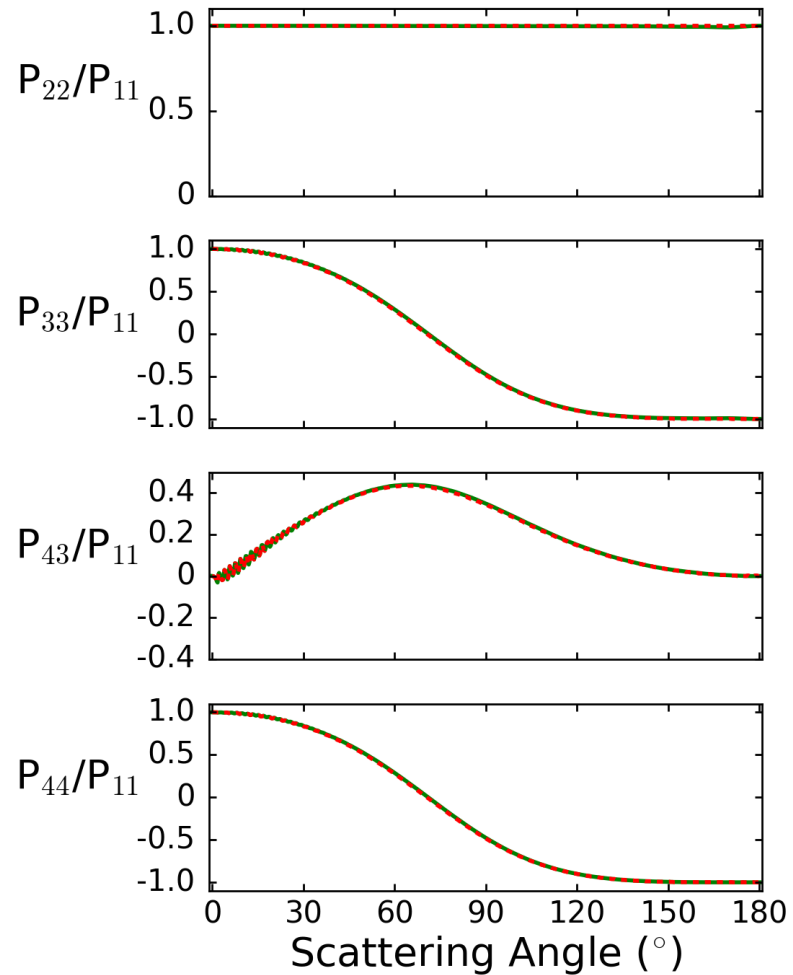
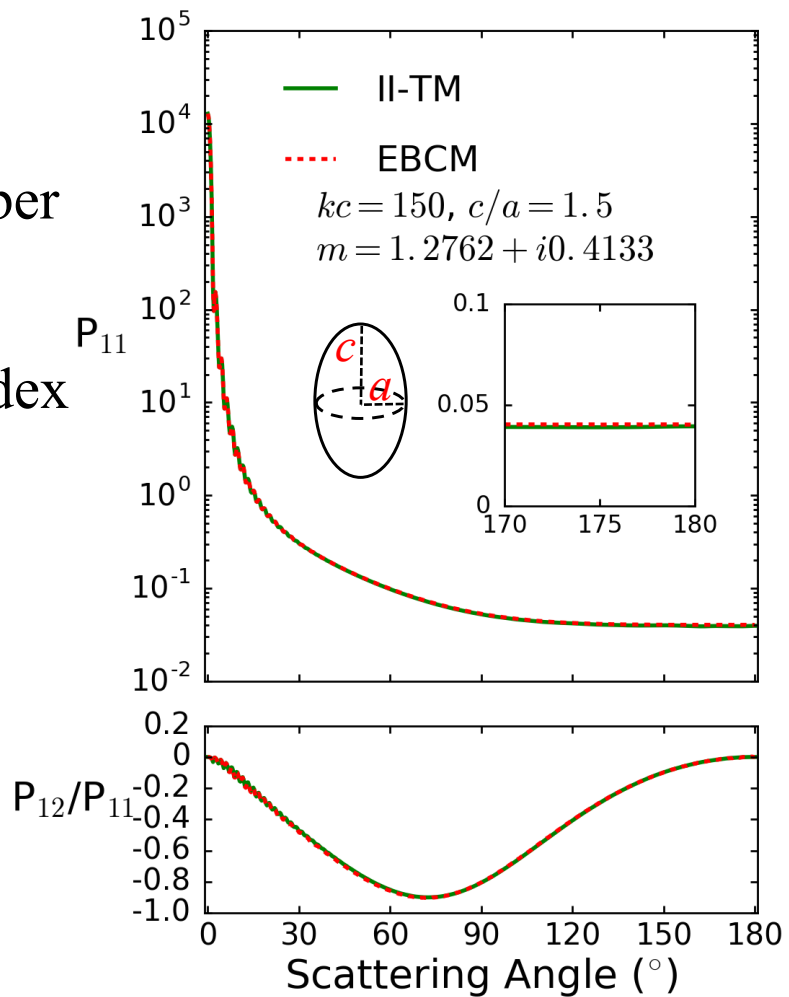
$m$ : complex  
refractive index



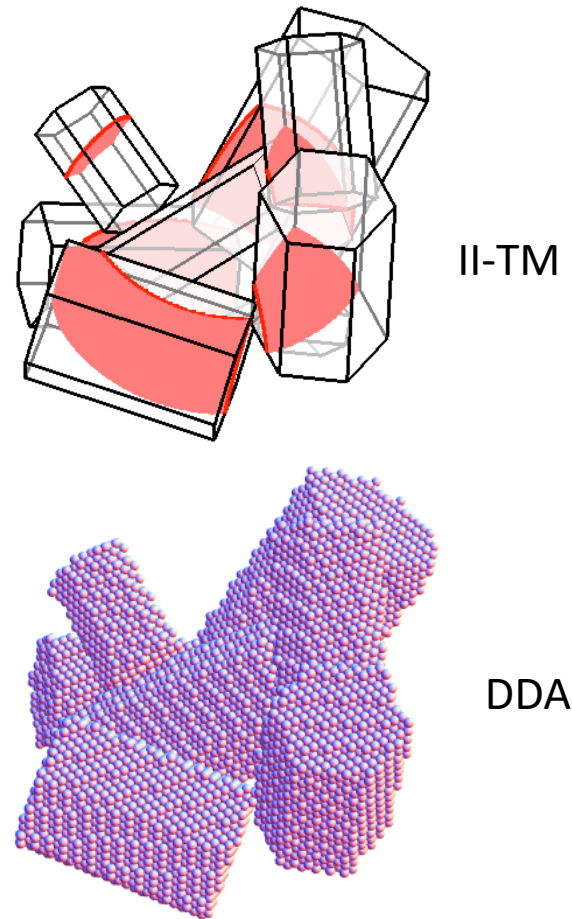
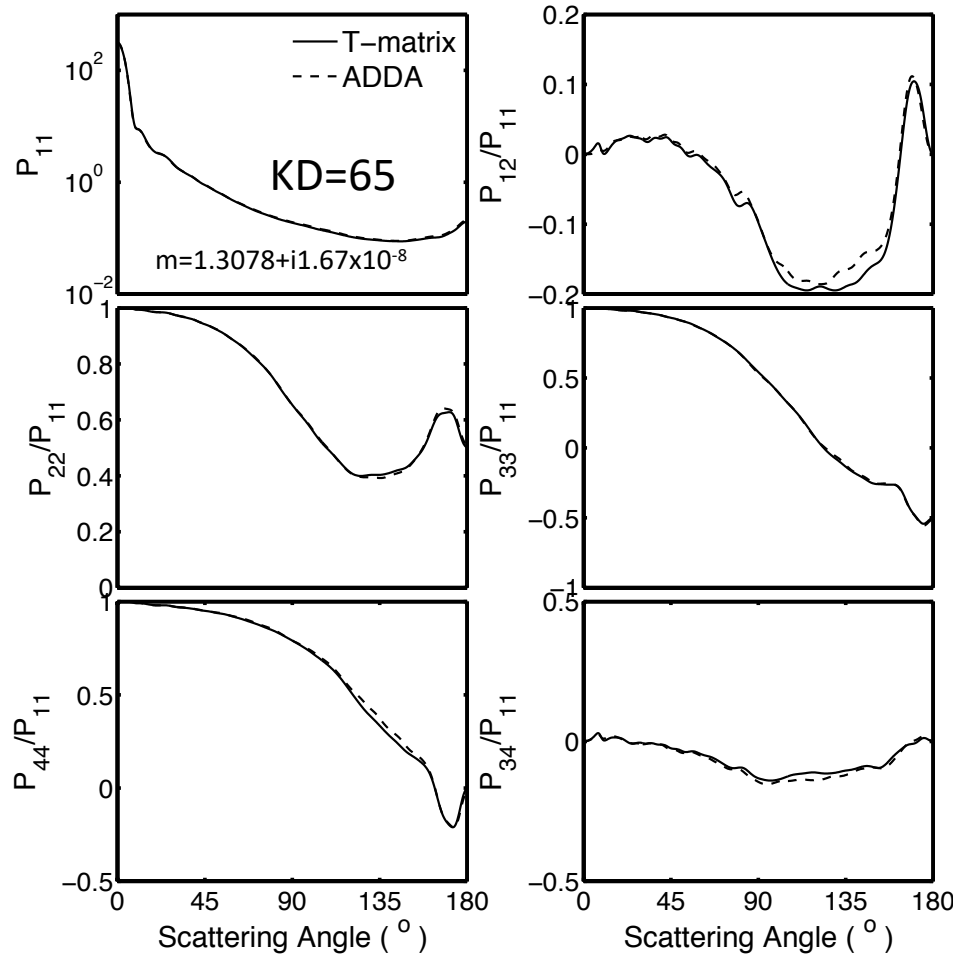
## II-TM and EBCM comparison: absorptive case

$k$ : wavenumber

$m$ : complex  
refractive index

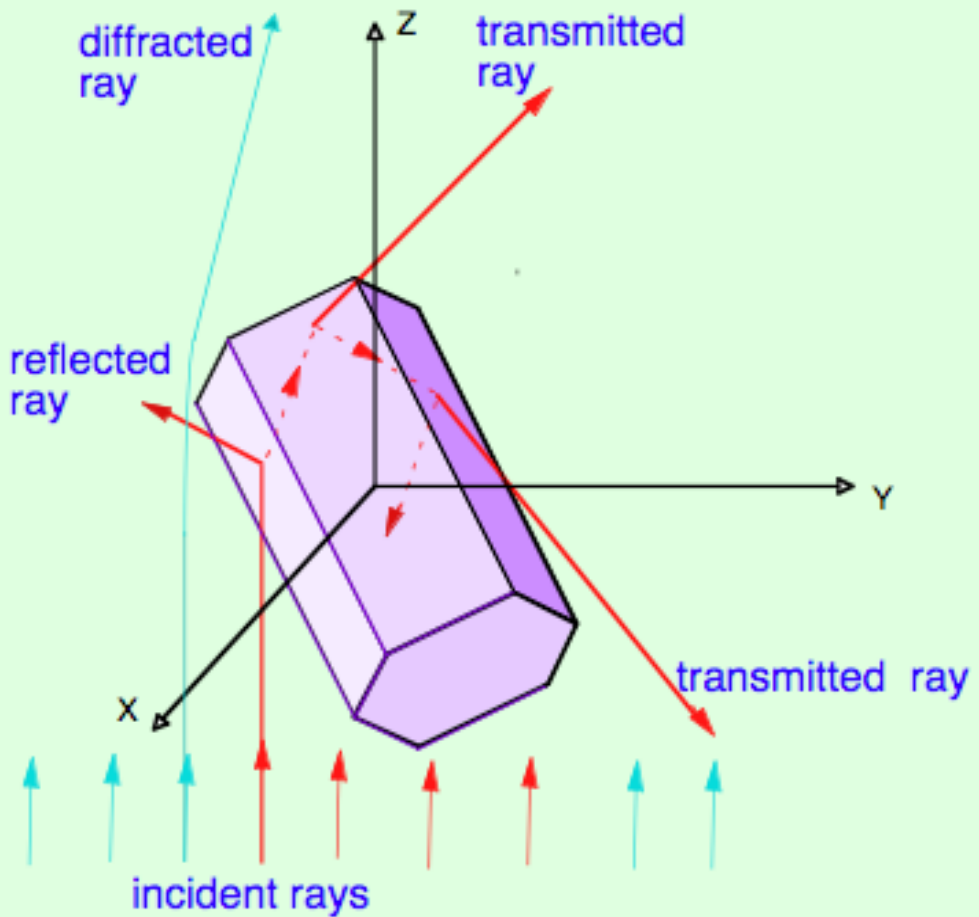


# Comparison between II-TM and DDA



In the DDA simulation, 1056 orientations with 128 scattering planes are set to achieve the randomness. [Bi and Yang \(2014\)](#).

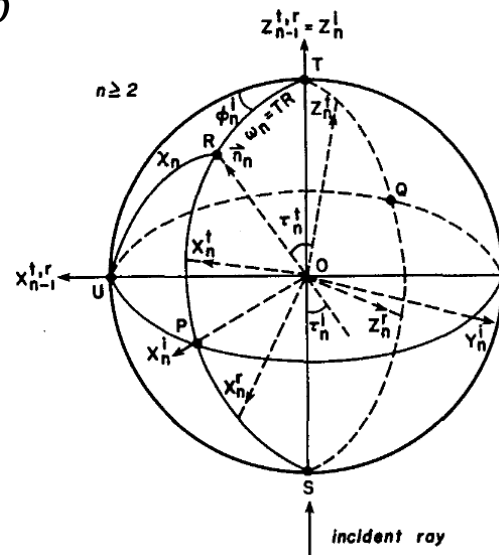
## Ray-Tracing Method for Light Scattering Calculation



## Conventional Geometric Optics

Method (Cai and Liou, 1982; Takano and Liou, 1989; Yang and Cai, 1991; Macke, 1992; ...)

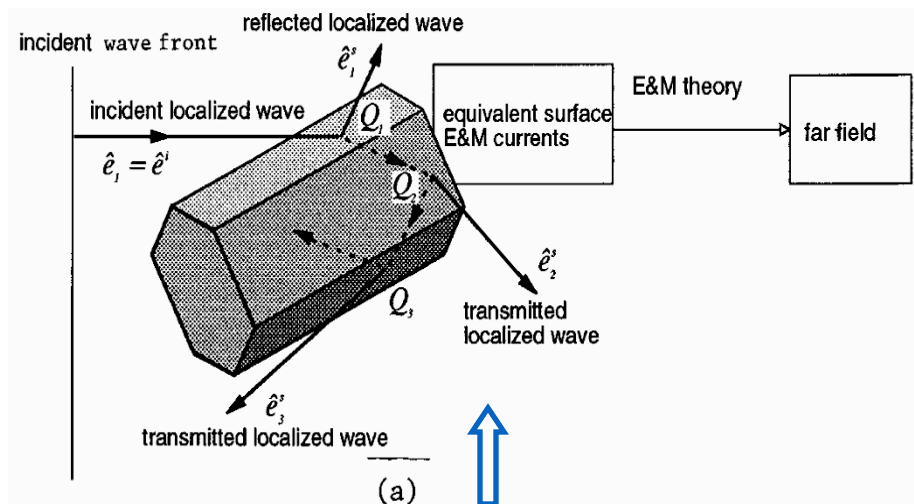
Cai, Q., and K. N. Liou, 1982: Polarized light scattering by hexagonal ice crystals: theory. *Appl. Op*



# Physical Geometric Optics Method

Yang and Liou (1996)

PGOMS – Surface-integral  
equation based

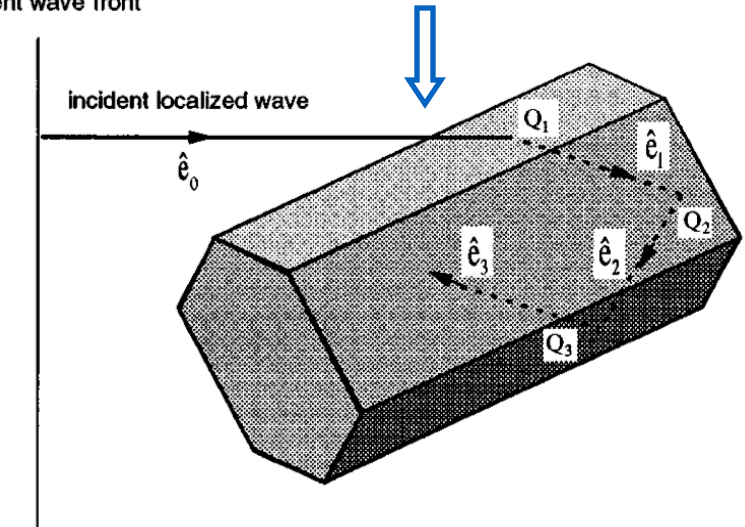


$$E_s(r)|_{kr \rightarrow \infty} = \frac{\exp(ikr)}{-ikr} \frac{k^2}{4\pi} \mathbf{n} \times \iint_S \{ \mathbf{n}_S \times \mathbf{E}(r') - \mathbf{n} \times [\mathbf{n}_S \times \mathbf{H}(r')] \} \times \exp(-ikn \cdot r') d^2 r',$$

Yang and Liou (1997)

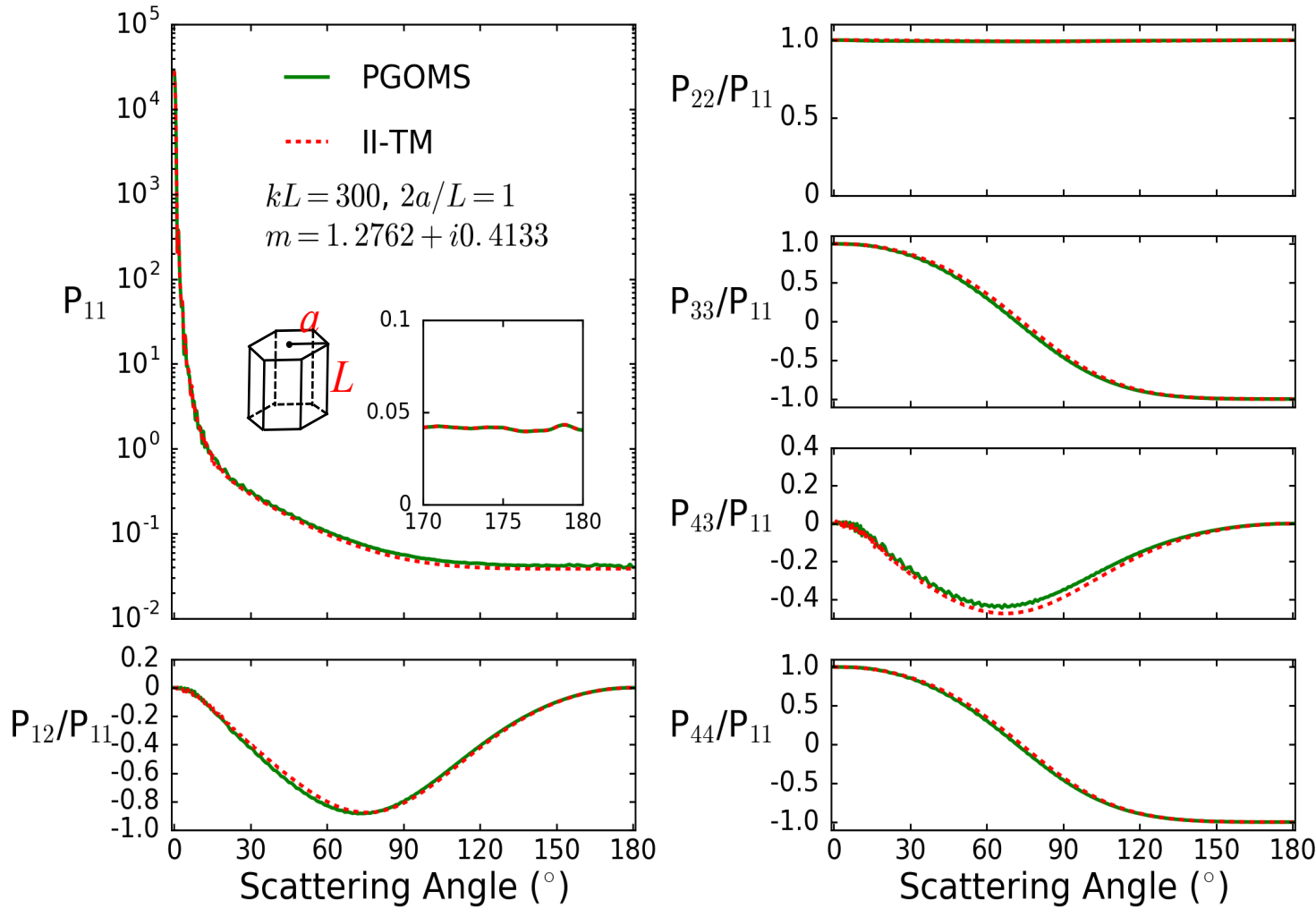
PGOMV – Volume-integral  
equation based

$$E_s(r) = \frac{k^2 \exp(ikr)}{4\pi r} \iiint_V [ \epsilon(r') - 1 ] [ \mathbf{E}(r') - \mathbf{n}[\mathbf{n} \cdot \mathbf{E}(r')] ] \exp(-ikn \cdot r') d^3 r'.$$



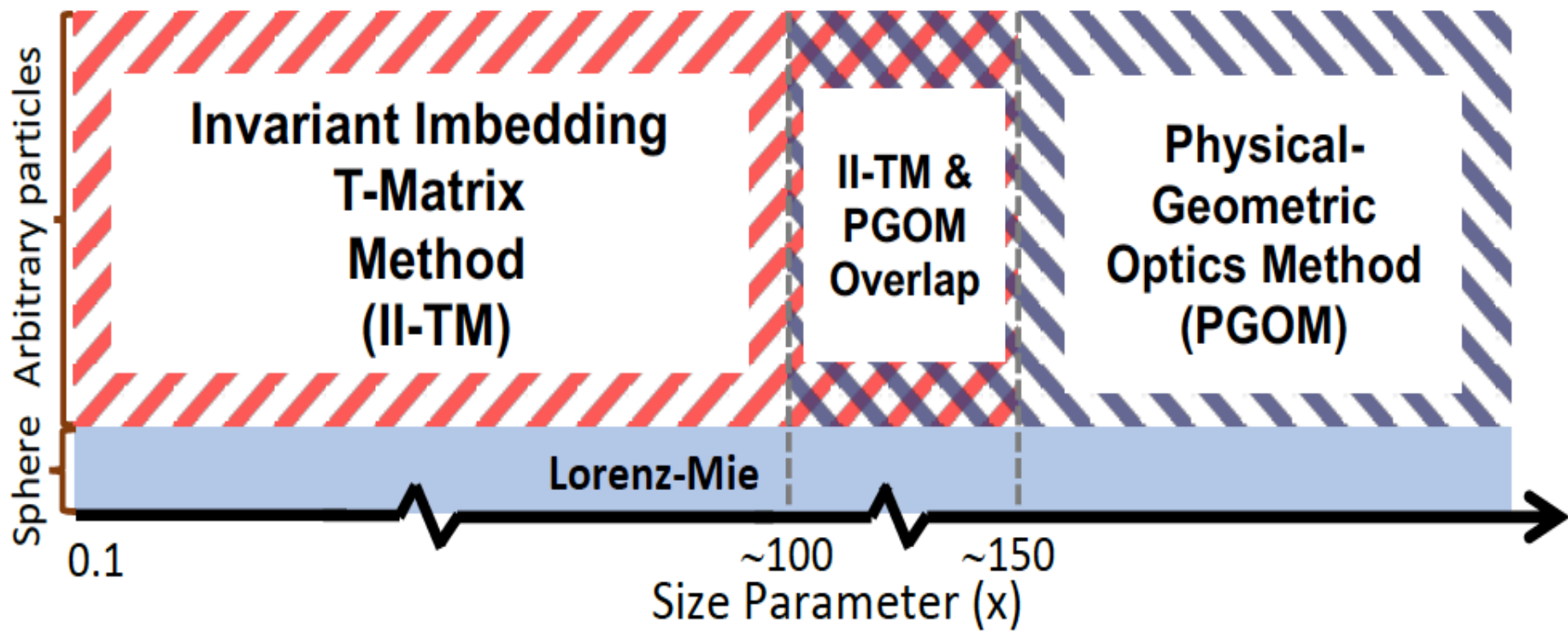
New improvements by our research group using computer graphics techniques (Yang et al. 2019)

# PGOMS vs II-TM



Comparison of the phase matrix elements computed by PGOMS and IITM. The particle is a hexagonal column with aspect ratio 1. The refractive index is  $1.2762+i0.4133$ , the ice refractive index at  $12\mu m$  wavelength. The inset plots show the  $P_{11}$  element for  $170^\circ$  -  $180^\circ$  scattering angles. The size parameter is  $kL=300$ .

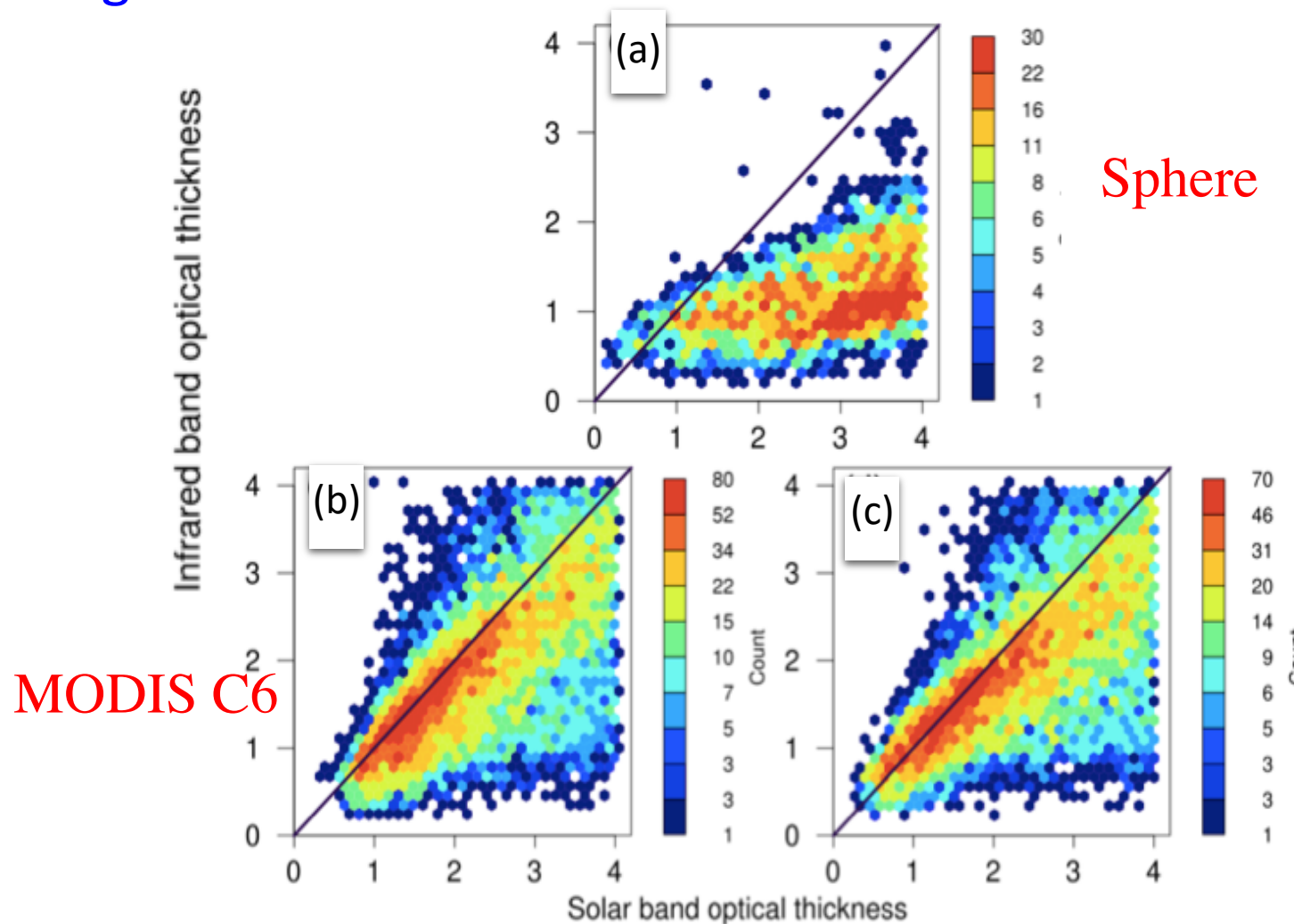
# Exact and approximated Method Converged



Yang et al., 2019, PIER

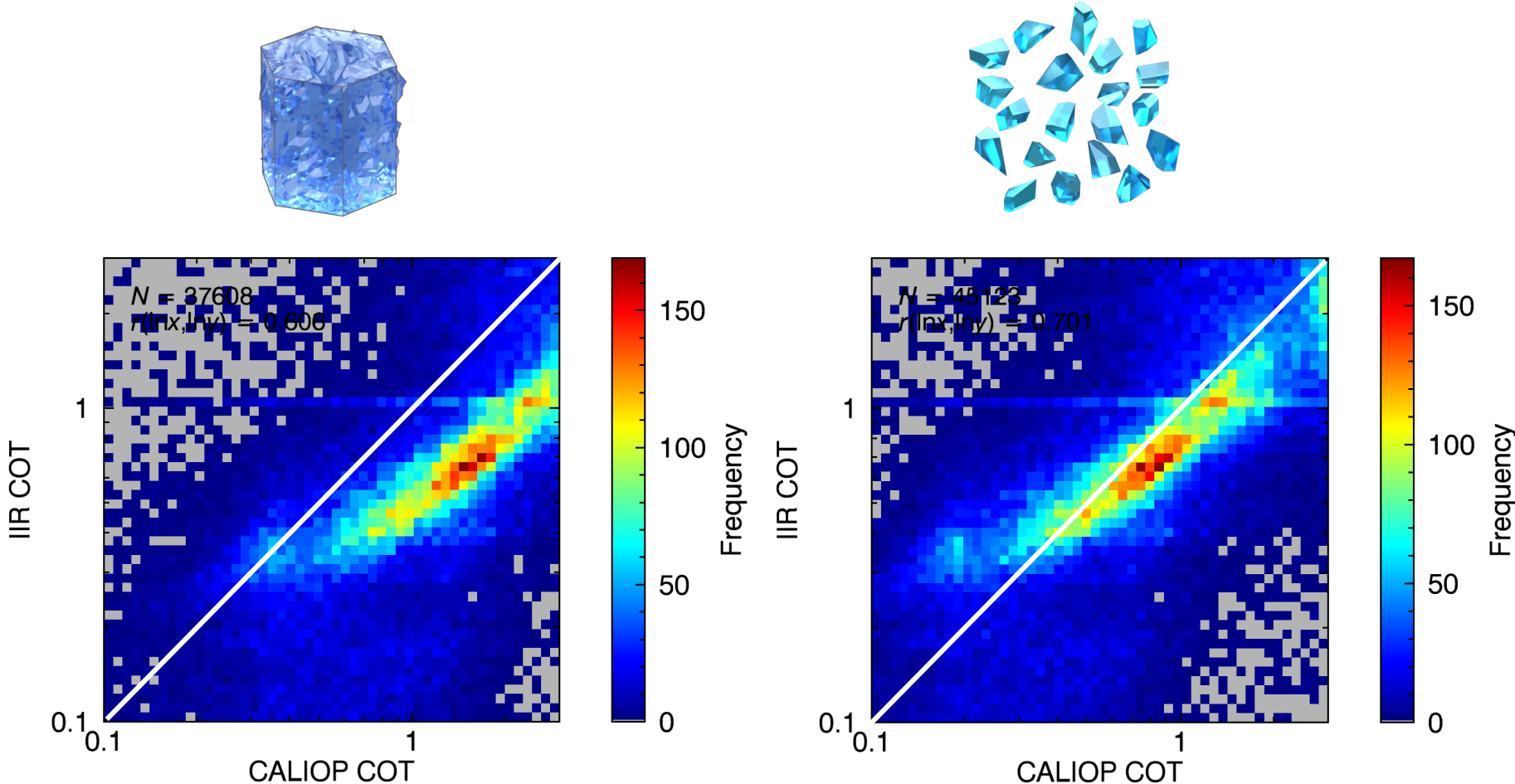
Unlike the previous modeling capabilities, this method is accurate in backscattering, leading to consistency for passive and active remote sensing applications.

# Spectral consistency between shortwave based retrieval and longwave based retrieval



Comparison of retrieved optical thickness values from a shortwave method (the Nakajima-King bi-spectral method) and a longwave method (the split-window technique). (a) Ice sphere, (b) MODIS Collection 6 model, and (c) Two-habit model (Potential CERES Edition 5 model)<sup>20</sup>.

# Consistency between active and passive remote sensing applications: Imaging Infrared Radiometer (IIR) vs CALIOP

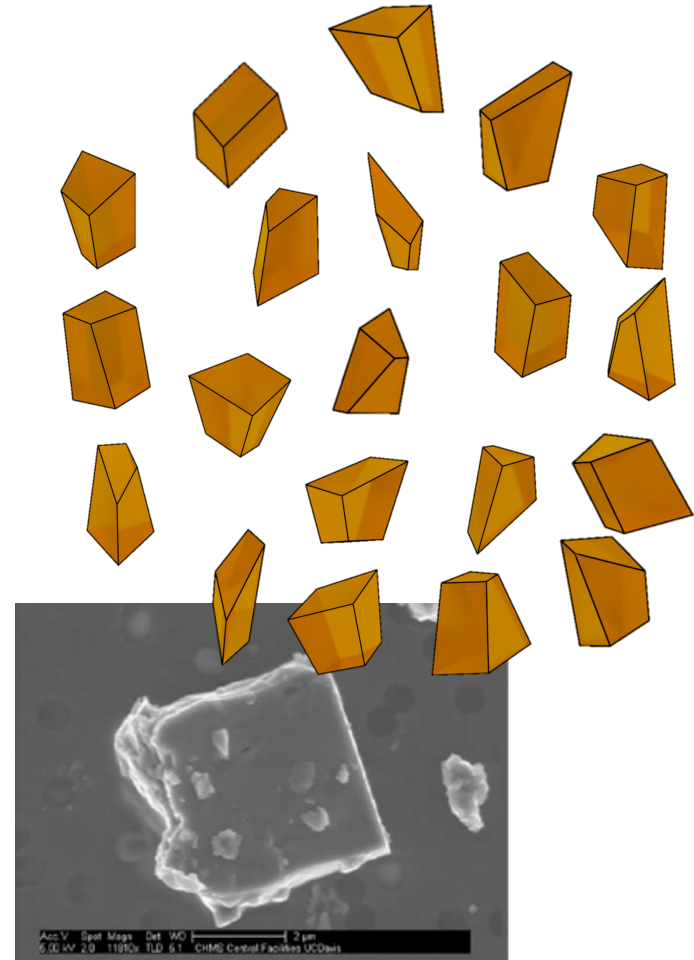


- Future THM shows better consistency between passive and active sensor-based COT retrievals

# Single-Scattering Property Database

- 20 irregular hexahedron ensemble dust model
  - Sphericity: 0.68–0.8
  - Size parameter: 0.03–1400
  - Realistic morphology
- Refractive index:
  - Real part: 1.37–1.6
  - Imaginary part:  $10^{-4}$ – $10^{-1}$
  - Obtained from literatures
- Spectral coverage
  - UV to shortwave (0.2–4  $\mu\text{m}$ )
  - Including three lidar wavelengths

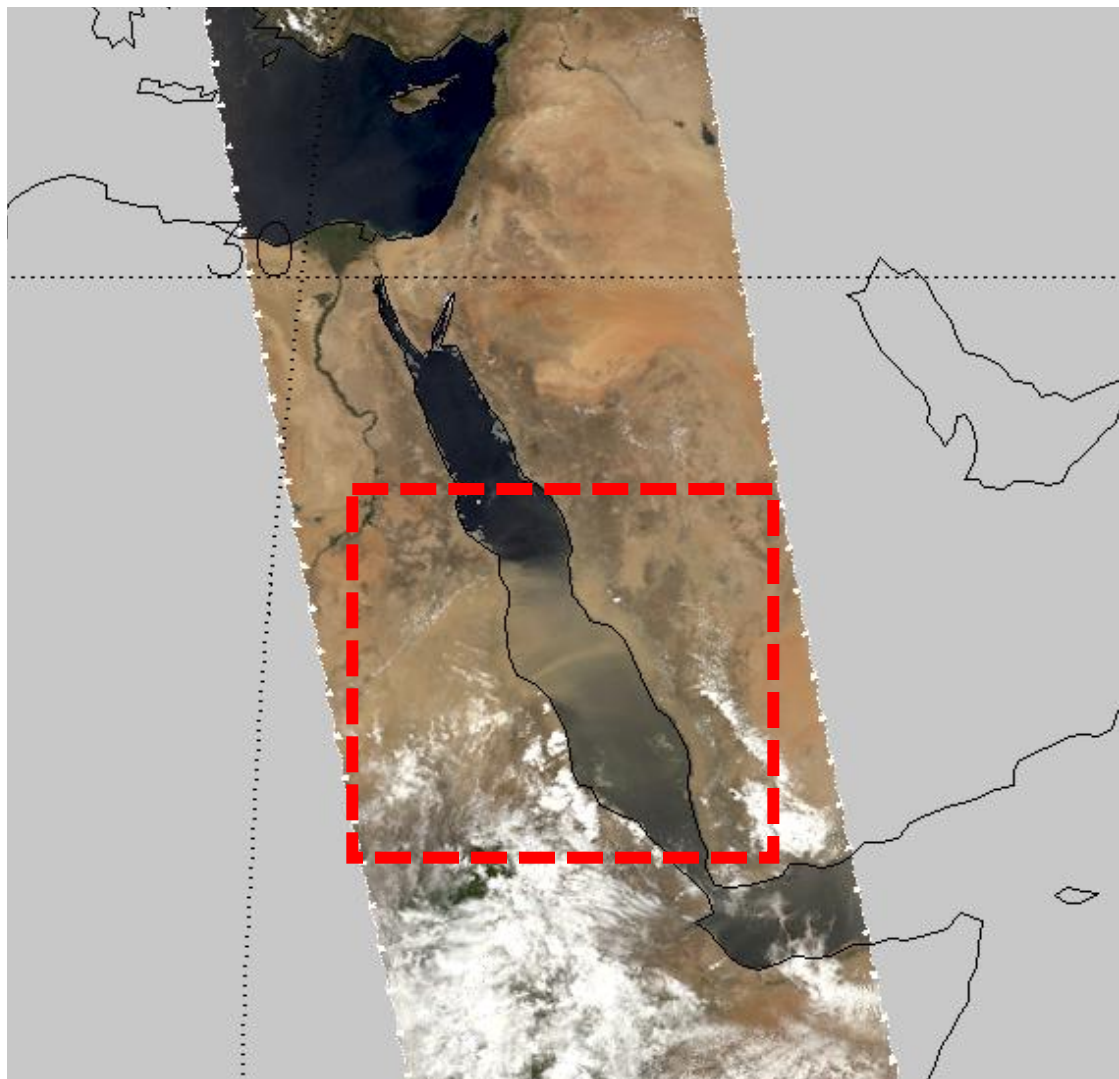
Example irregular hexahedron particles



Reid et al., 2003

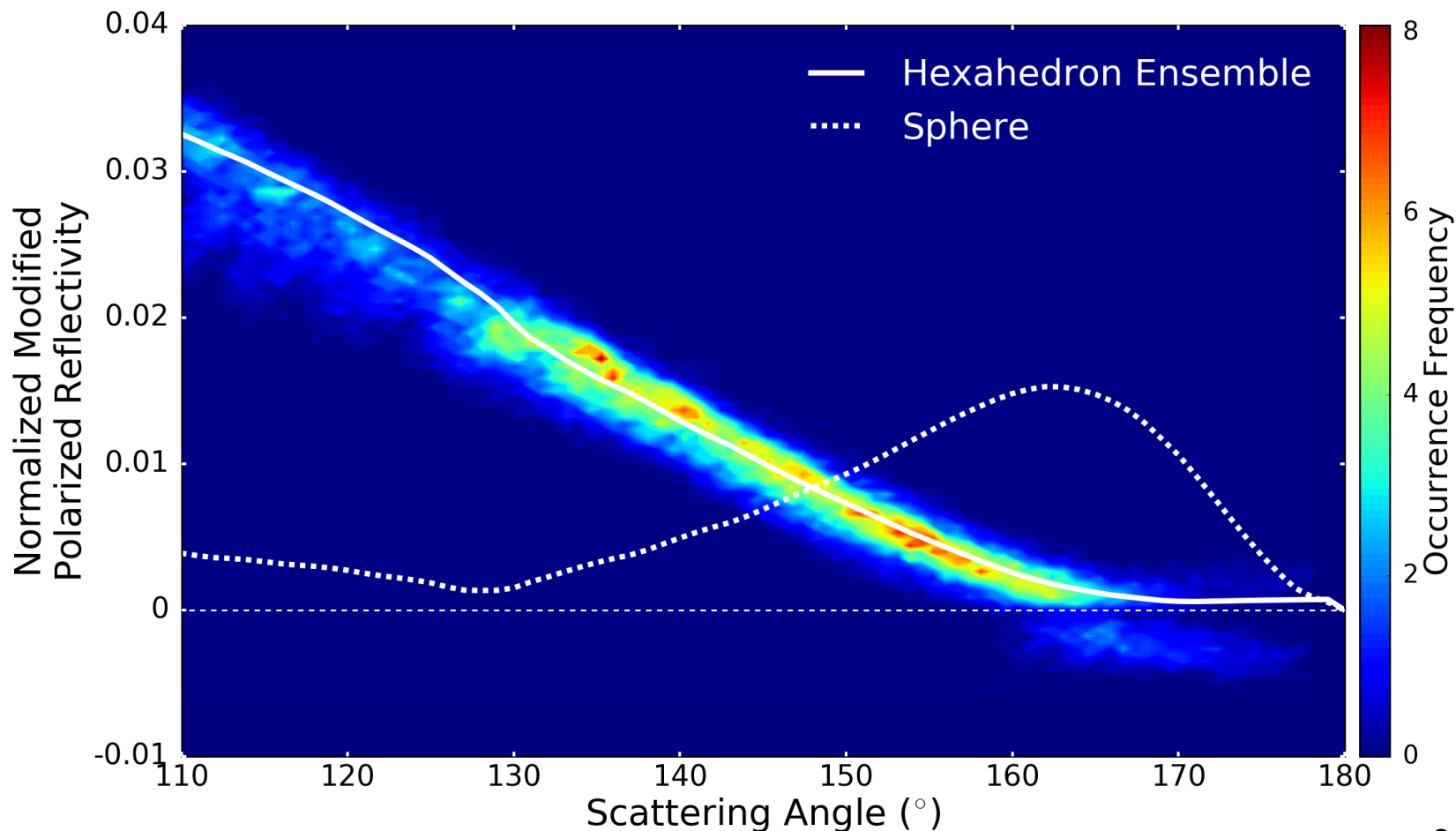
# Remote sensing application

PARASOL data over red sea



# Consistency between observation and simulation

Compared the simulation with PARASOL data (865 nm band)



# Flexible Dust Database

## Input files

- Maximum dimension bins
- Wavelength bins
- Refractive index



## Output files

- Optical properties
- Physical properties
- Phase matrix elements

### (1) Prepare input files

Size.txt

Maximum Dimension

2.00000E-02

2.25000E-02

2.50000E-02

Wavelength.txt

.

Wavelength

2.00000E-01

2.40000E-01

2.80000E-01

RefrIdx.txt

.

RealPart

1.50000E+00

1.52000E+00

1.55000E+00

ImaginaryPa

2.47000E-02

1.35000E-02

9.40000E-03

.

.

### (2) Run Fortran code

TAMUdust2020.f90

- User-friendly interface
- Fortran code: ~600MB

### (3) Provide a dust property database

isca.dat

Qext

2.01000E+00

2.02000E+00

1.00000E+00

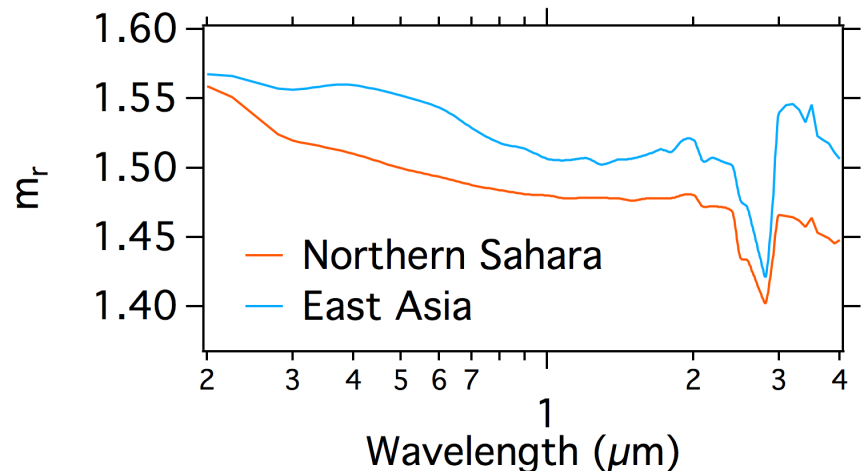
P???.dat

.

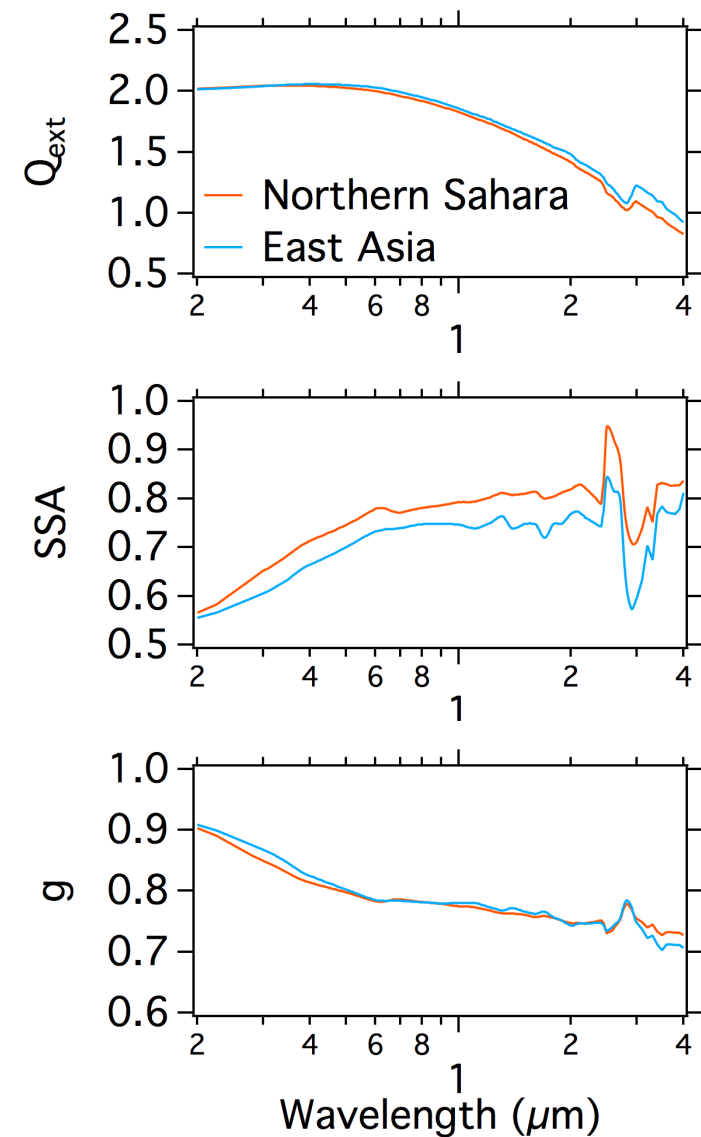
2.01000E+00

# Dust Single-Scattering Properties

Refractive Index

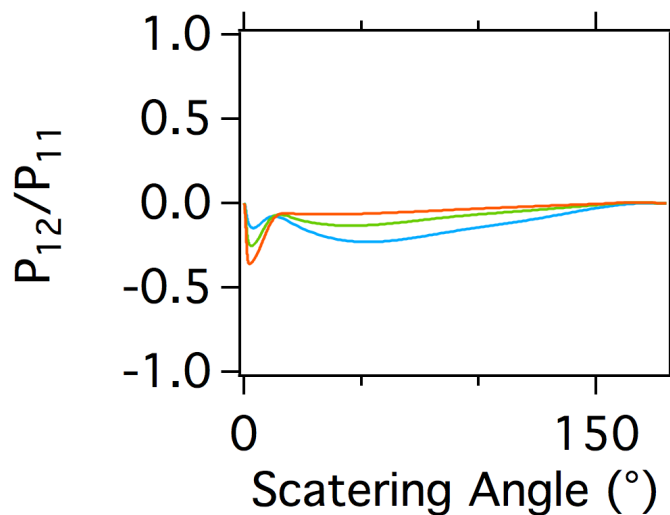
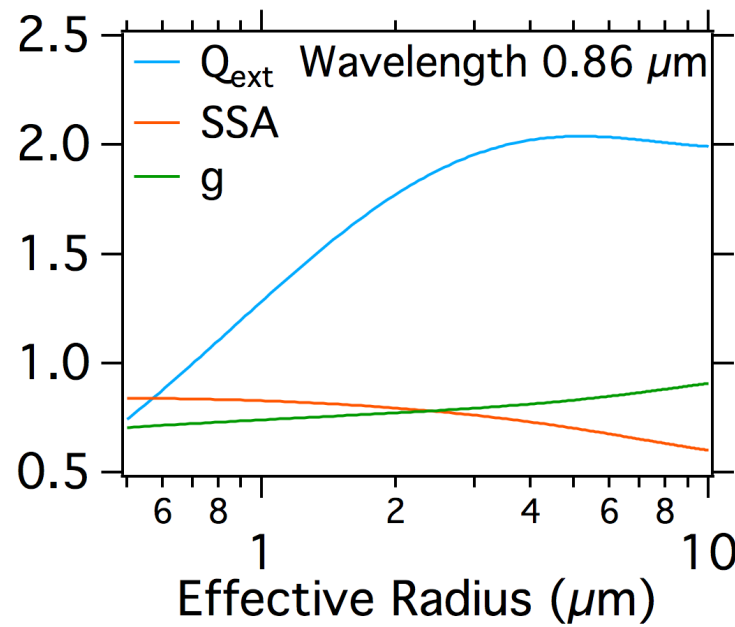
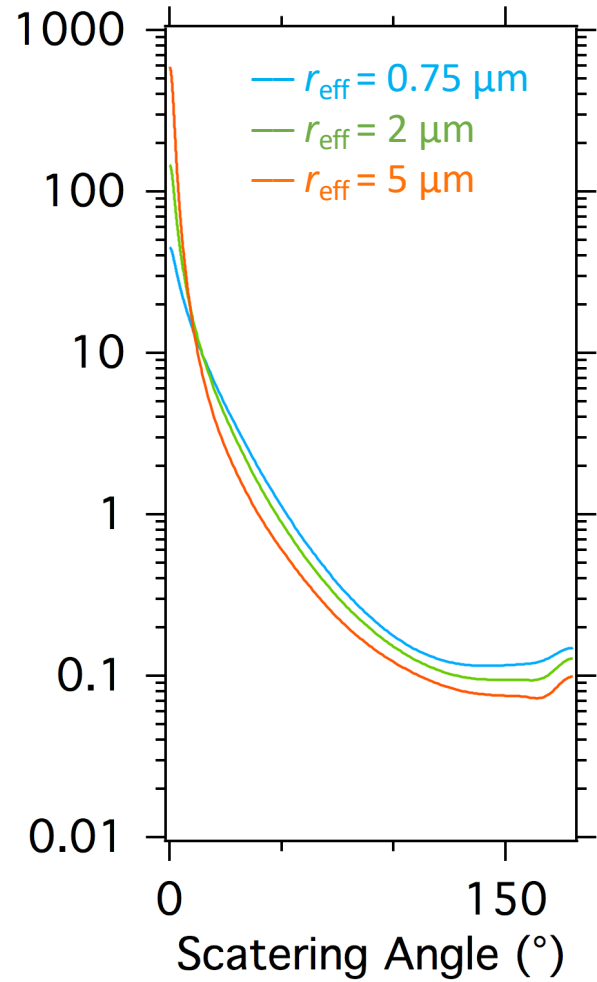


Single-scattering Properties



# Dust Single-Scattering Properties

Northern Sahara Model



- A robust vector radiative transfer model for **active (lidar based)** remote sensings application (**with Yong X. Hu**)
- A fast vector radiative transfer model for **passive** remote sensing applications (**with Michael King, Steven Platnick, Xu Liu**)

**Ding, J., P. Yang, M. D. King, S. Platnick, X. Liu, K. G. Meyer, C. Wang, 2019:** A fast vector radiative transfer model for atmosphere-ocean coupled system, *J. Quantitative Spectroscopy & Rad. Transfer*,  
<https://doi.org/10.1016/j.jqsrt.2019.106667>

$$u \frac{\partial \mathbf{I}(\tau, u, \phi)}{\partial \tau} = \mathbf{I} - \frac{\varpi}{4\pi} \int_{-1}^1 du' \int_0^{2\pi} d\phi' \mathbf{I}(\tau, u', \phi') \mathbf{P}(\tau, u', \phi', u, \phi) - (1 - \varpi) \mathbf{B}(T(\tau))$$

Phase matrix:  $\mathbf{P}(\tau, u, u', \varphi - \varphi') = \mathbf{L}(\pi - \eta_2) \mathbf{F}(\tau, \Theta) \mathbf{L}(-\eta_1)$

$$\mathbf{P}(\Theta) = \mathbf{P}^f(\Theta) + \mathbf{P}^d(\Theta)$$

$$\mathbf{I}(\tau, \mu, \phi) = \mathbf{I}^f(\tau^f, \mu, \phi) + \mathbf{I}^d(\tau^d, \mu, \phi)$$



$$u \frac{\partial \mathbf{I}^d(\tau^d, u, \phi)}{\partial \tau^d} = \mathbf{I}^d - \frac{\varpi^d}{4\pi} \int_{-1}^1 d\phi' \mathbf{I}^d(\tau^d, u', \phi') \mathbf{P}^d(\tau^d, u, \phi, u', \phi') - (1 - \varpi^d) \mathbf{B}(T(\tau^d))$$

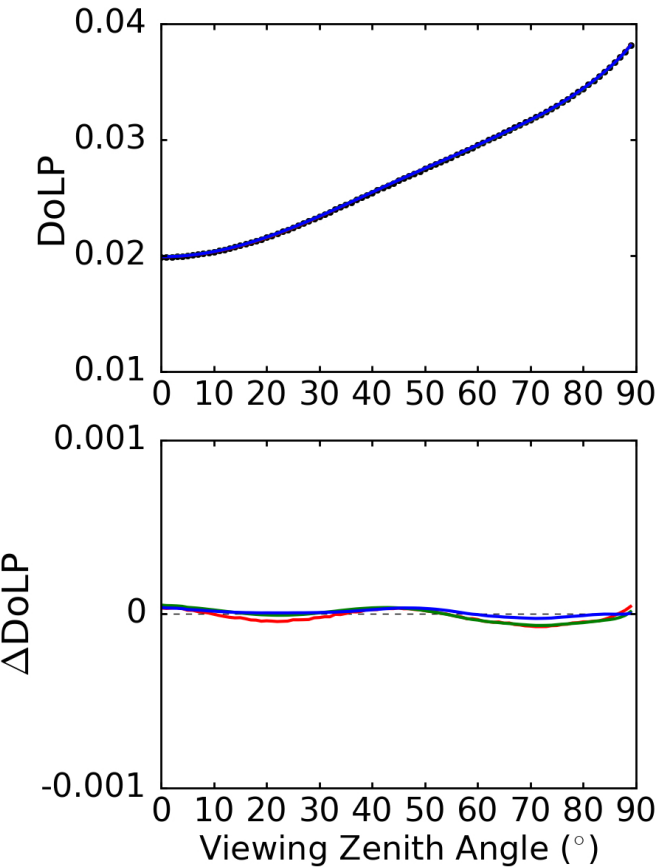
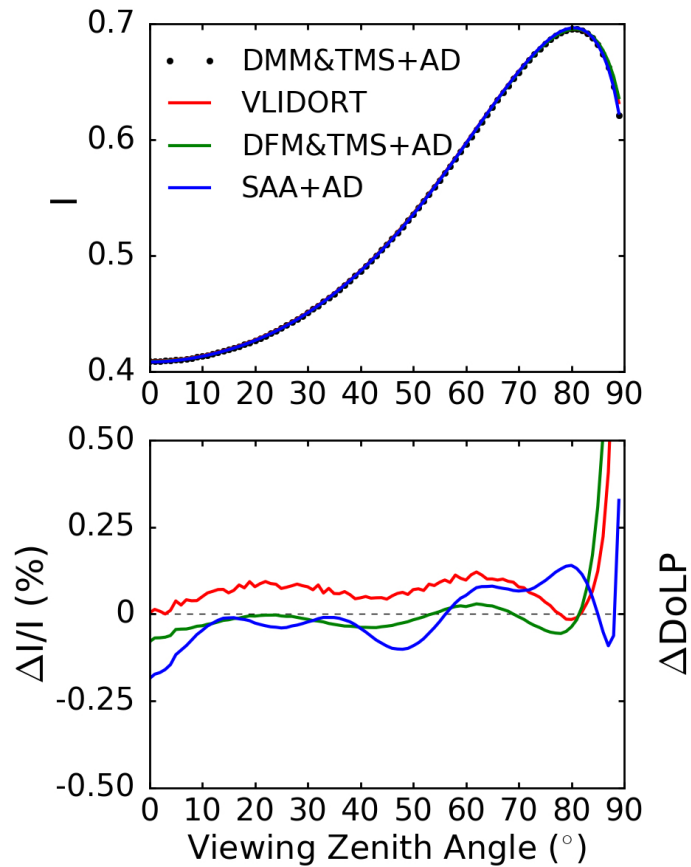
Adding-doubling (AD)

$$u \frac{\partial \mathbf{I}^f(\tau^f, u, \phi)}{\partial \tau^f} = \mathbf{I}^f - \frac{\varpi^f}{4\pi} \int_{-1}^1 d\phi' \mathbf{I}^f(\tau^f, u', \phi') \mathbf{P}^f(\tau^f, u, \phi, u', \phi')$$

$$I^f(\tau^f, \mu, \phi) \approx \frac{1}{2\pi} \frac{F}{\sqrt{V_{nx} V_{ny}}} \exp \left( -\frac{n_x^2}{2V_{nx}} - \frac{n_y^2}{2V_{ny}} \right)$$

Small-angle approximation (SAA)

# Reflected Radiation



An ice cloud layer

Ice cloud COT=5  
 $r = 30.0 \mu\text{m}$

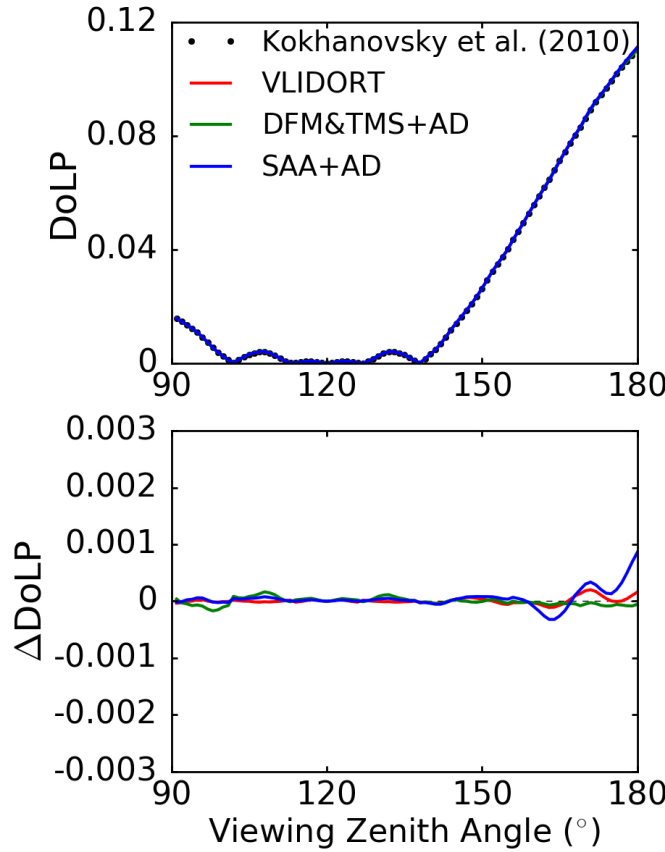
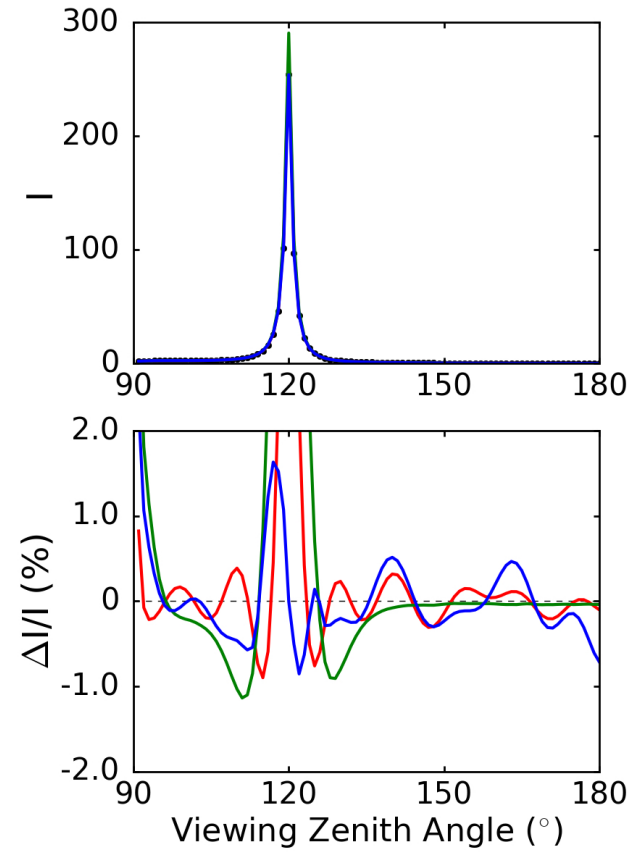
DMM&TMS+AD: Adding-doubling with Delta-M truncation and TMS single-scattering correction

DFM&TMS+AD: Adding-doubling with Delta-Fit truncation and TMS single-scattering correction

Wavelength:  $0.865 \mu\text{m}$

Incident zenith angle:  $60^\circ$   
Relative azimuth angle:  $90^\circ$

# Transmitted Radiation



An aerosol layer

Aerosol AOT=0.3262

$r = 2.46 \mu\text{m}$

Wavelength:  $0.412 \mu\text{m}$

Incident zenith angle:  $60^{\circ}$   
Relative azimuth angle:  $0^{\circ}$

# Regression-based Method for Gas Absorption

Channel-averaged optical thickness (CAOT):

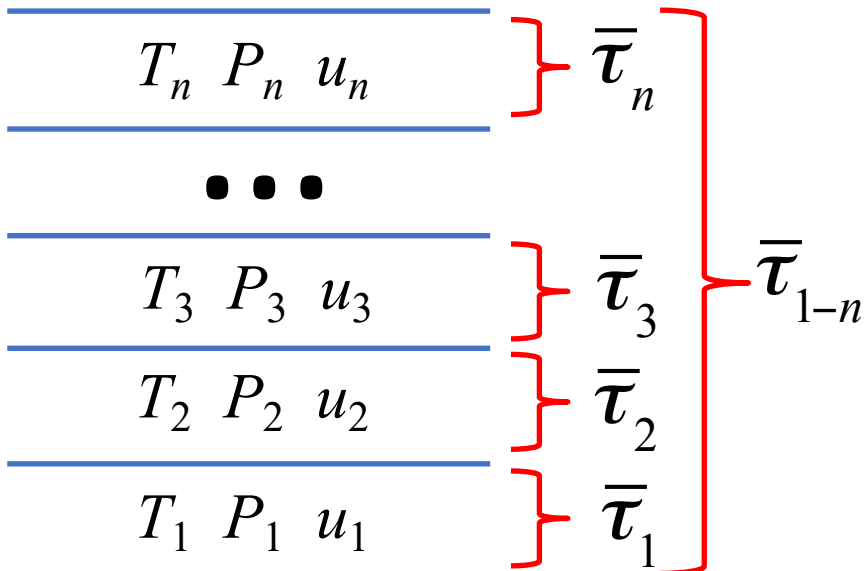
$$\bar{\tau}_{i \sim j} \equiv -\ln \bar{t}_{i \sim j}$$

- Pressure
- Temperature
- Gas concentration

Absorptive gases: H<sub>2</sub>O CO<sub>2</sub> O<sub>3</sub> N<sub>2</sub>O CO CH<sub>4</sub> O<sub>2</sub> N<sub>2</sub>

# Regression-based Method for Gas Absorption

## Previous methods



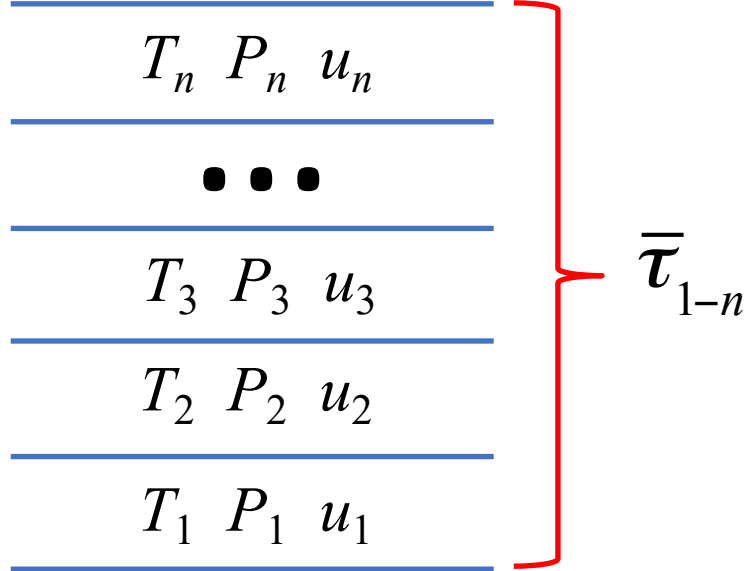
$u$ : gas concentration

$P$ : pressure

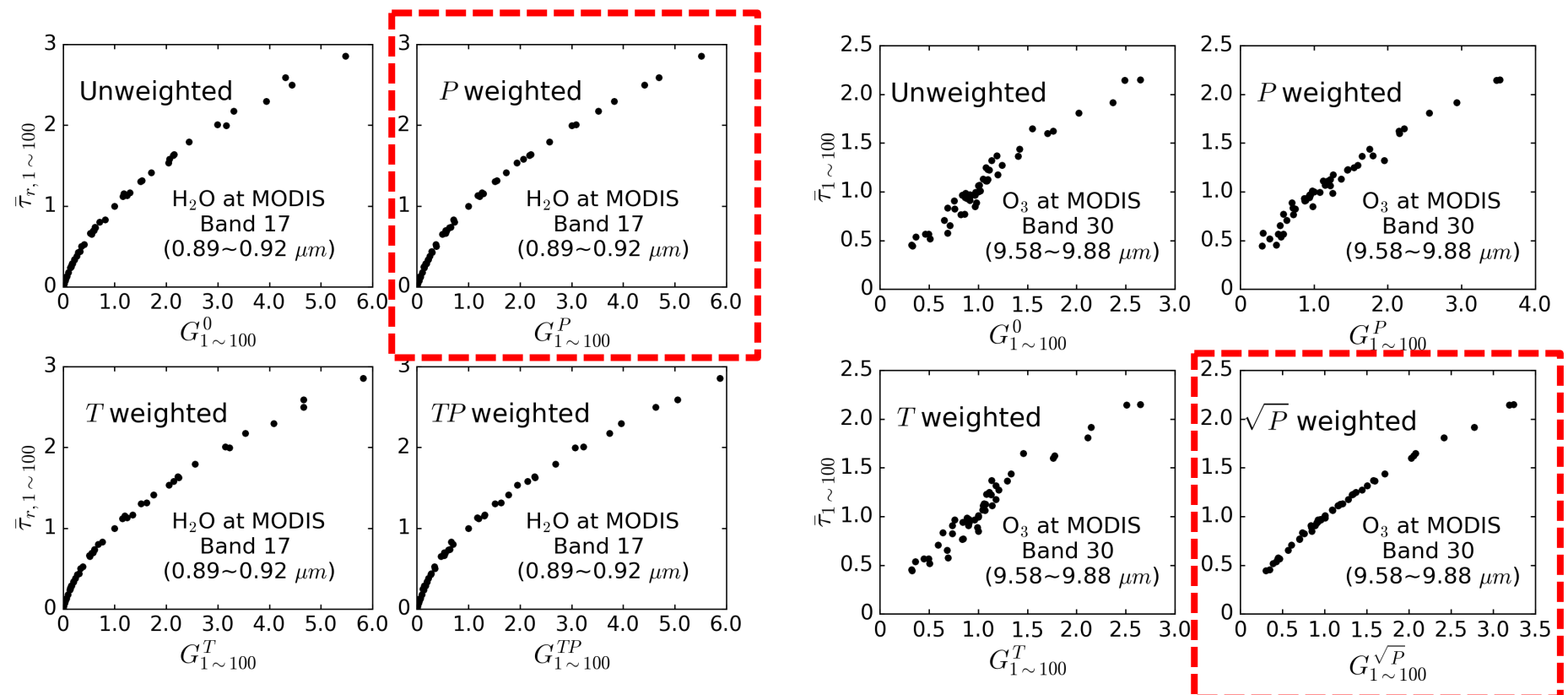
$T$ : temperature

$n$ : number of layers

## Our method

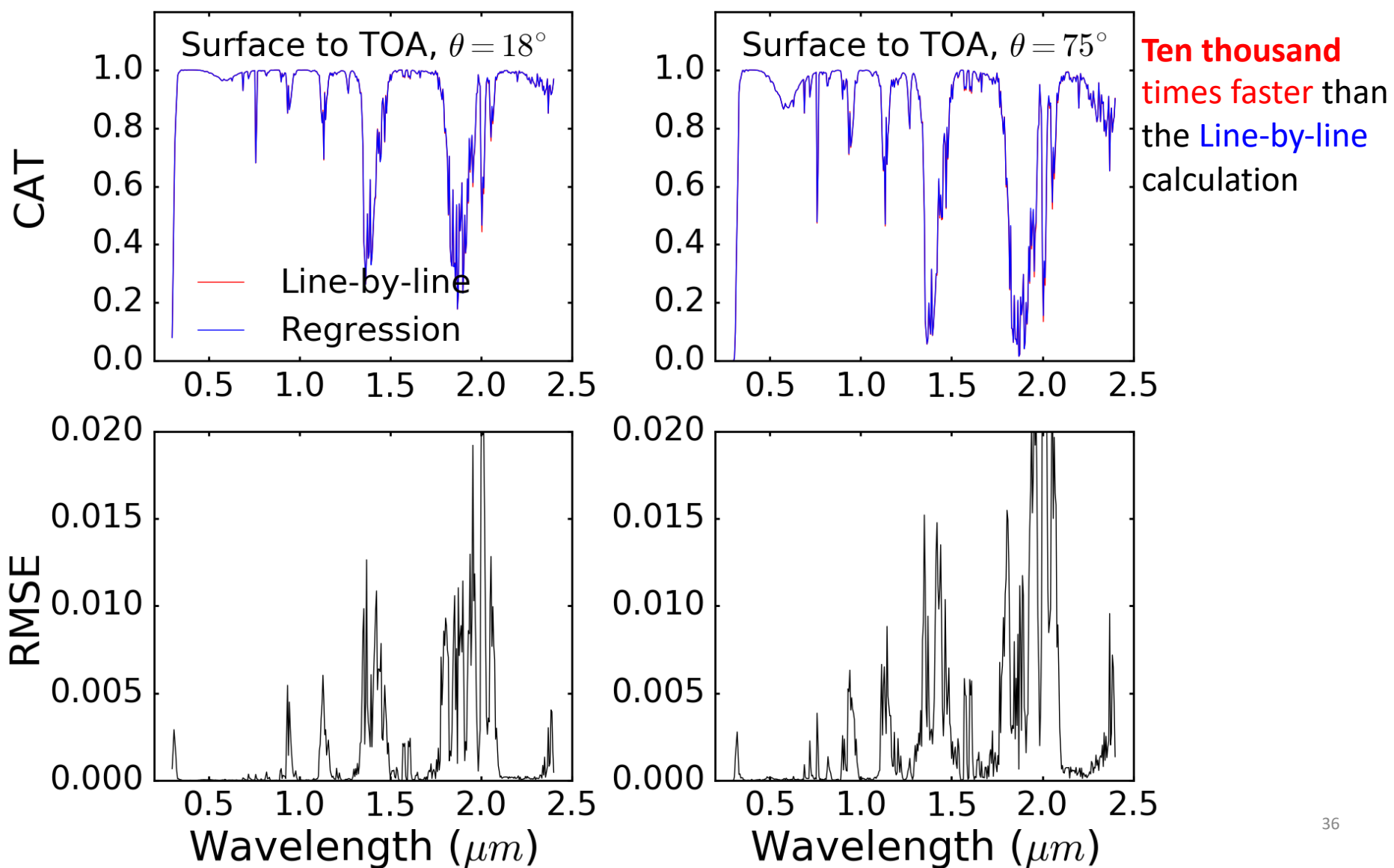


# Regression-based Method for Gas Absorption

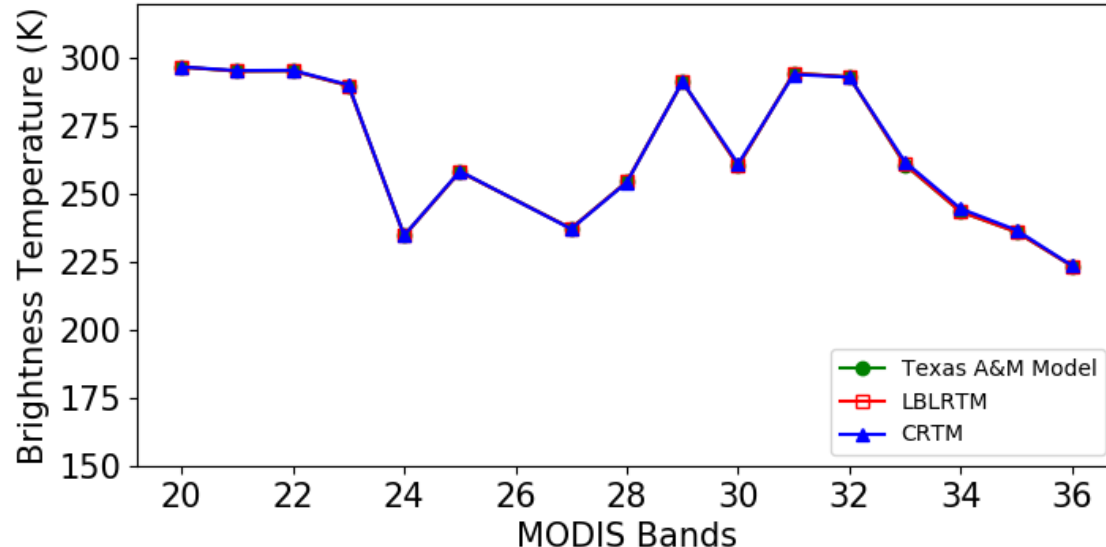


$$\bar{\tau}_{1-n} = b_3 (G_{1-n})^{3\gamma} + b_2 (G_{1-n})^{2\gamma} + b_1 (G_{1-n})^\gamma + b_0$$

# Hyperspectral Channel Averaged Transmissivity

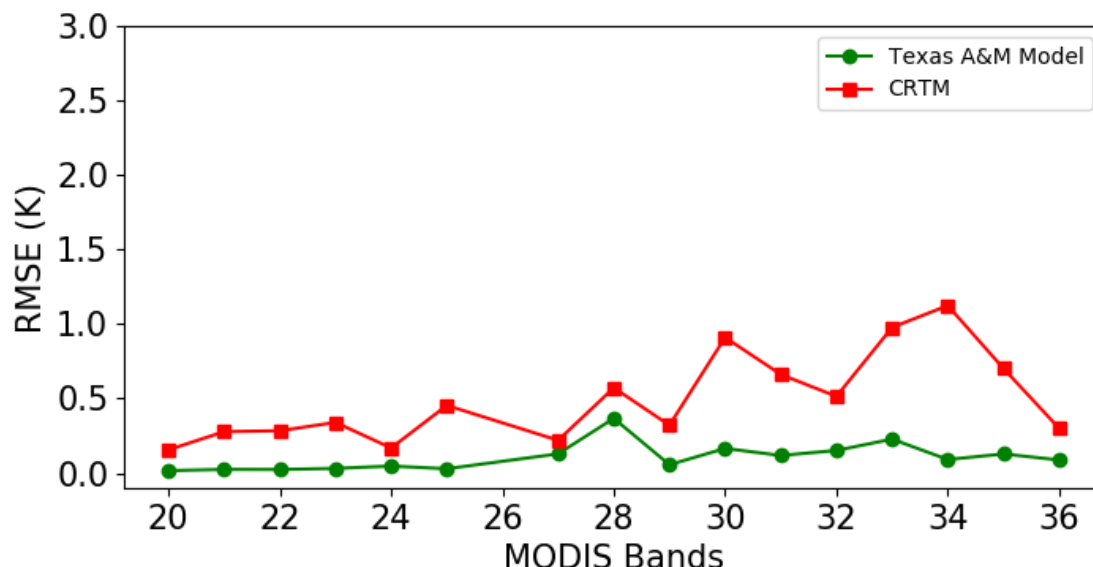


# Clear Sky TOA Brightness Temperature



Ten thousand times faster than the Line-by-line calculation;

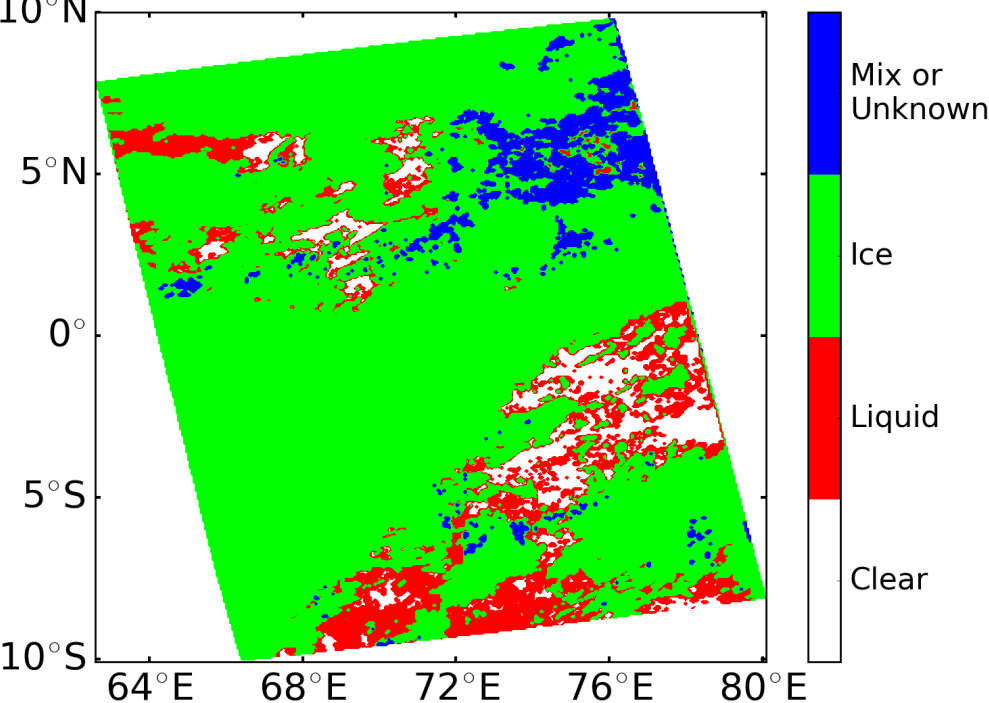
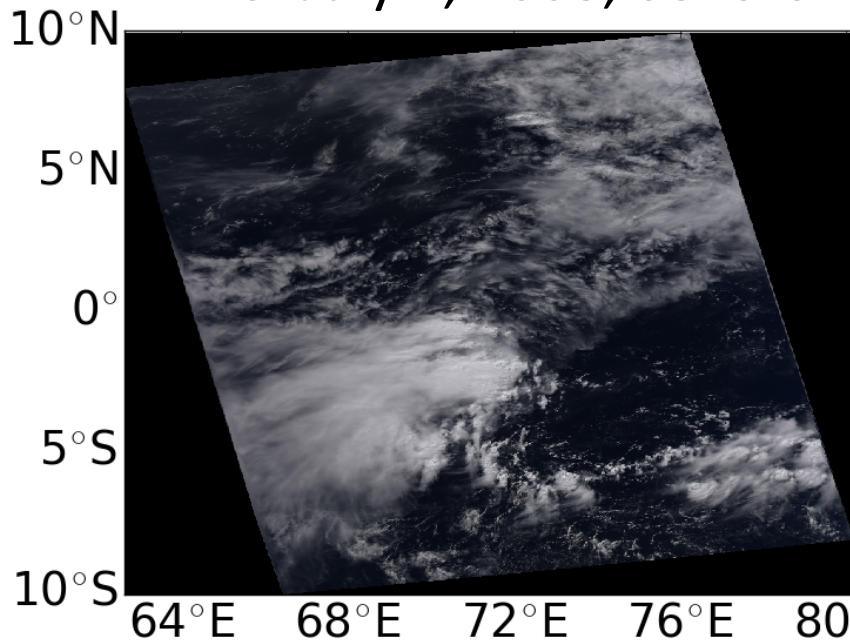
Two times faster than 32-point Correlated K-distribution (CKD) method.



# Satellite Radiance Simulations

Simulation region: Indian Ocean, southwest of Sri Lanka

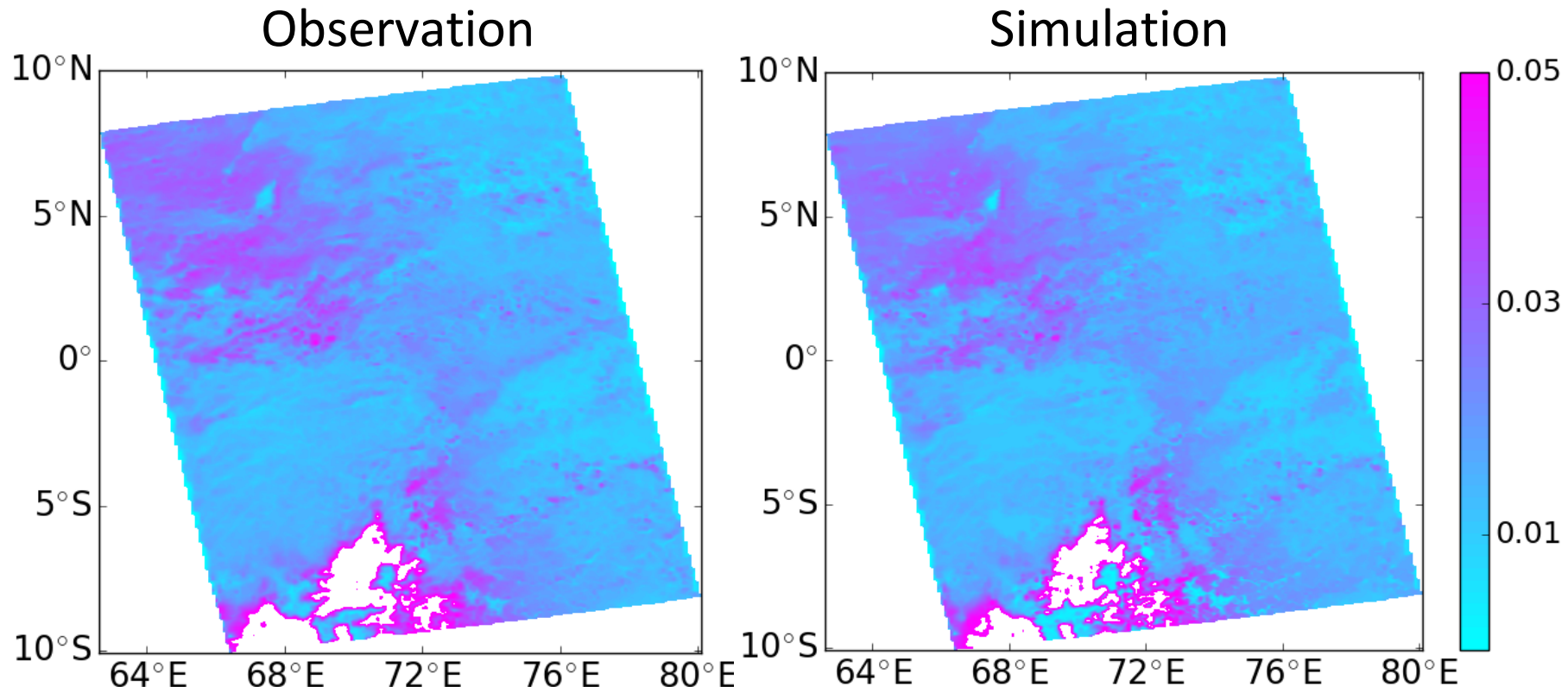
Time: July 1, 2008, 0845 UTC



Input data

- MODIS Collection 6 cloud product
- MERRA-2 atmospheric profile data

# POLDER Polarized Reflectance



- Polarized reflectance at  $0.865 \mu\text{m}$  simulated with MODIS cloud product is consistent with collocated POLDER observation.

# Oceanic *Inherent Optical Properties*

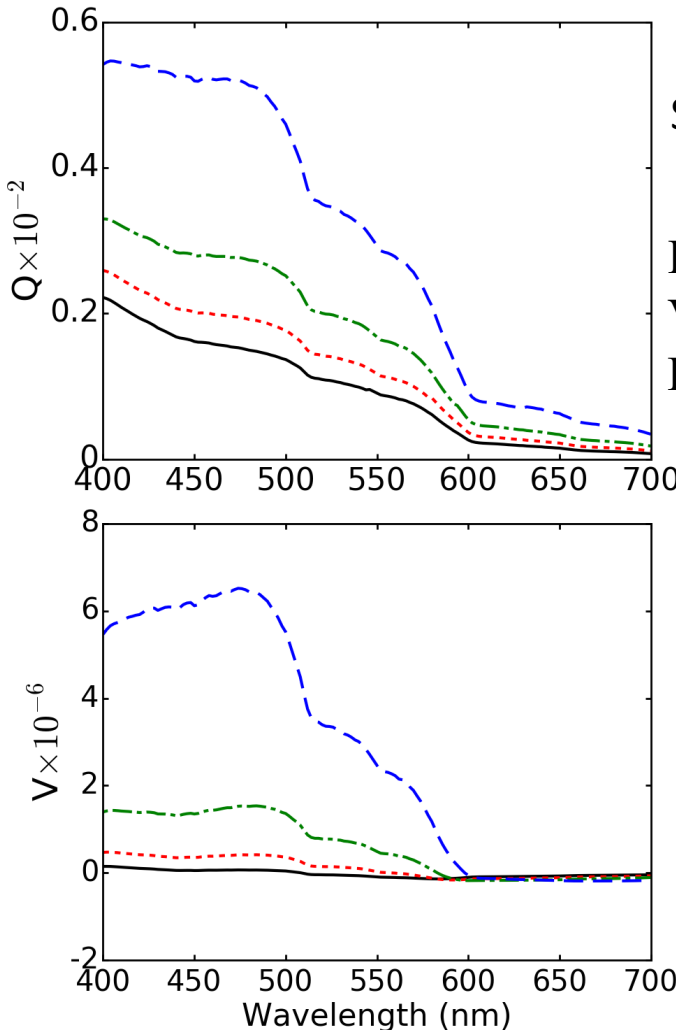
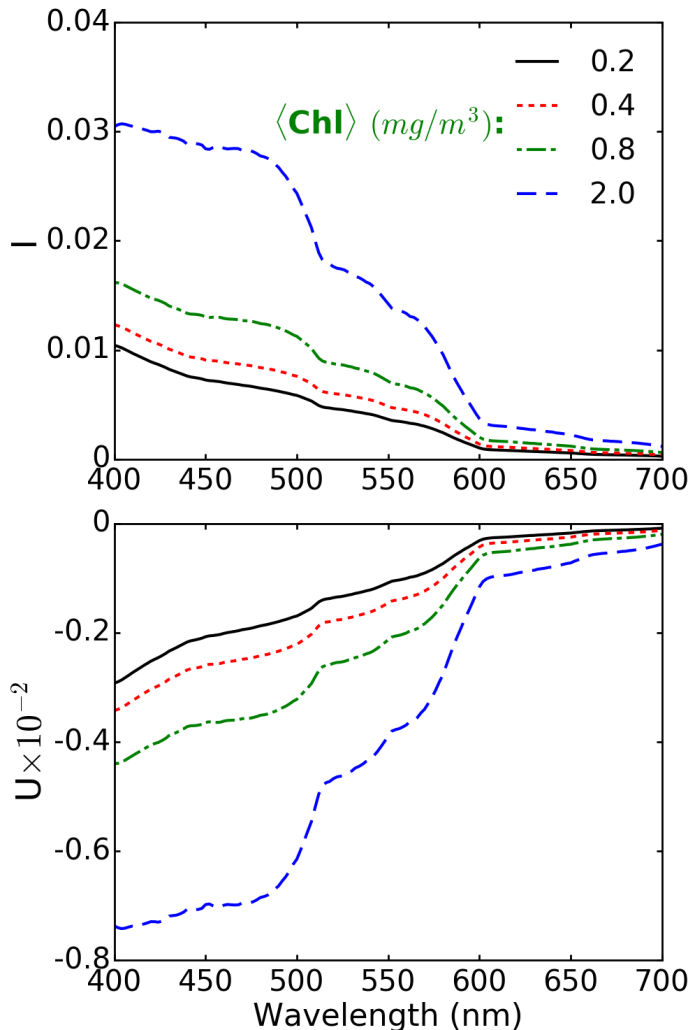
Inherent optical properties (IOP):

- Absorption coefficient
- Scattering coefficient
- Scattering matrix

Ocean model constituents:

- Pure water
- Colored dissolved organic matter (CDOM)
- Phytoplankton
- Non-algae particles (NAPs)

# Spectral Stokes Parameters above Ocean Surface



Ocean depth: 10 m  
Surface wind speed: 7 m/s  
Incident zenith angle: 60°  
Viewing zenith angle: 40°  
Relative azimuth angle: 90°

# Summary

- Developed a database of dust single-scattering properties
  - 20 hexahedron ensemble dust model
  - Various sizes, refractive indices, and degrees of sphericity
  - A flexible, user-friendly dust database
  - Useful for lidar + passive polarimetric simulations
- Developed a fast vector radiative transfer model for passive remote sensing applications.
  - A fast regression-based gas absorption
  - An accurate and efficient two-component method (SAA+AD) for multiple scattering
  - An air-sea interface
  - An ocean model